Geosci. Model Dev. Discuss., https://doi.org/10.5194/gmd-2018-155
Manuscript under review for journal Geosci. Model Dev.
Discussion started: 16 July 2018

Geoscientific Model Development
Open Access
Discussions

Description and basic evaluation of simulated mean state, internal variability, and climate sensitivity in MIROC6

Hiroaki Tatebe[1], Tomoo Ogura[2], Tomoko Nitta[3], Yoshiki Komuro[1], Koji Ogochi[1], Toshihiko Takemura[4], Kengo Sudo[5], Miho Sekiguchi[6], Manabu Abe[1], Fuyuki Saito[1], Minoru Chikira[3], Shingo Watanabe[1], Masato Mori[7], Nagio Hirota[2], Yoshio Kawatani[1], Takashi Mochizuki[1], Kei Yoshimura[3], Kumiko Takata[2], Ryouta O'ishi[3], Dai Yamazaki[8], Tatsuo Suzuki[1], Masao Kurogi[1], Takahito Kataoka[1], Masahiro Watanabe[3], and Masahide Kimoto[3]

1: Japan Agency for Marine-Earth Science and Technology, Yokohama, Japan

2: National Institute for Environmental Studies, Tsukuba, Japan

3: Atmosphere and Ocean Research Institute, University of Tokyo, Kashiwa, Japan

4: Research Institute for Applied Mechanics, Kyushu University, Kasuga, Japan

5: Graduate School of Environmental Studies, Nagoya University, Nagoya, Japan

6: Tokyo University of Marine Science and Technology, Tokyo, Japan

7: Research Center for Advanced Science and Technology, University of Tokyo, Tokyo, Japan

8: Institute of Industrial Sciences, University of Tokyo, Tokyo, Japan

Corresponding author: Hiroaki Tatebe
Project team for advanced climate modeling, Japan Agency for Marine-Earth Science and Technology
3173-25 Showa-machi, Kanazawa-ku, Yokohama, Kanagawa 236-0001, Japan
E-mail: tatebe@jamstec.go.jp

Abstract

The sixth version of the Model for Interdisciplinary Research on Climate (MIROC), called MIROC6, was cooperatively developed by a Japanese modeling community. In the present manuscript, simulated mean climate, internal climate variability, and climate sensitivity in MIROC6 are evaluated and briefly summarized in comparison with the previous version of our climate model (MIROC5) and observations. The results show that overall reproducibility of mean climate and internal climate variability in MIROC6 is better than that in MIROC5. The tropical climate systems (e.g., summertime precipitation in the western Pacific and the eastward propagating Madden-Julian Oscillation) and the mid-latitude atmospheric circulations (e.g., the westerlies, the polar night jet, and troposphere-stratosphere interactions) are significantly improved in MIROC6. These improvements can be attributed to the newly implemented parameterization for shallow convective processes and to the directly resolved stratosphere. While there are significant differences in climates and variabilities between the two models, the effective climate sensitivity of 2.5 K remains the same because the differences in radiative forcing and climate feedback tend to offset each other. With an aim towards contributing to the sixth phase of the Coupled Model Intercomparison Project, designated simulations tackling a wide range of climate science issues, as well as seasonal-to-decadal climate predictions and future climate projections, are currently ongoing using MIROC6.

Geosci. Model Dev. Discuss., https://doi.org/10.5194/gmd-2018-155
Manuscript under review for journal Geosci. Model Dev.
Discussion started: 16 July 2018

1 Introduction

As the global warming due to increasing emissions of the anthropogenic greenhouse gases progresses, it is anticipated, or has been already observed that global and regional patterns of climatic mean atmospheric temperature, circulation, and precipitation will drastically change (e.g., Neelin et al., 2006; Zhang et al., 2007; Bengtsson et al., 2009; Andrews et al., 2010; Scaife et al., 2012) and that extreme weather events such as heatwaves, droughts, and extratropical cyclones will increase (e.g., Mizuta et al., 2012; Sillmann et al., 2013; Zappa et al., 2013). Corresponding to the atmospheric changes under the global warming, the sea levels will rise due to the thermal expansion of sea water and ice-sheet melting in the polar continental regions (e.g., Church and White, 2011; Bamber and Aspinall, 2013). Additionally, ocean acidification due to absorption of atmospheric carbon dioxide (CO_2) and changes in carbon-nitrogen cycles are expected to lead to the loss of Earth biodiversity (e.g., Riebesell et al., 2009; Rockström, et al. 2009; Taucher and Oschlies, 2011; Watanabe et al., 2017). Societal demands for information on the global and regional climate changes have increased significantly worldwide in order to meet information requirements for political decision making related to mitigation and adaptation to the global warming.

The Intergovernmental Panel on Climate Change (IPCC) has continuously published the assessment reports (ARs) in which a comprehensive view of past, present, and future climate changes on various timescales, including the centennial global warming, are synthesized (IPCC 2007; 2013). Together with observations, climate models have been contributing to the IPCC-ARs through a broad range of numerical simulations, especially, future climate projections after the twenty-first century. However, there are many uncertainties in future climate projections and the range of uncertainties has not been narrowed by an update of the IPCC reports. The uncertainties are arising from imperfections of climate models in representing micro- to global-scale physical and dynamical processes in sub-systems of the Earth's climate and their interactions. To reduce the uncertainties and errors in climate projections and predictions, utilizing observations, extracting essences of physical processes in the real climate, and sophisticating physical parameterizations of climate models, which represent unresolved sub-grid scale phenomena, are necessary. A state-of-the-art climate model which can represent various processes in the Earth's climate system is a powerful tool for deeper understanding the Earth's climate system.

One of Japanese climate models, which is called MIROC (Model for Interdisciplinary Research on Climate), has been cooperatively developed at the Center for Climate System Research (CCSR; the precursor of a part of the Atmosphere and Ocean Research Institute), the University of Tokyo, the Japan Agency for Marine-Earth Science and Technology (JAMSTEC), and the National Institute for Environmental Studies (NIES). Utilizing MIROC, our Japanese climate modelling group has been tackling a wide range of climate science issues and seasonal-to-decadal climate predictions and future climate projections. At the same time, by providing simulation data, we have been participating to the third and fifth phases of the Coupled Model Intercomparison Projects (CMIP3 and CMIP5; Meehl et al. 2007; Taylor et al. 2011) which have been contributing to the IPCC-ARs by synthesizing multi-model ensemble datasets.

In the years up to the IPCC fifth assessment report (IPCC-AR5), we have developed four versions of MIROC, three of which (MIROC3m, MIROC3h, and MIROC4h) have almost the same dynamical and physical packages, but different resolutions. MIROC3m (K-1 model developers, 2004) is a medium-resolution model consisting of T42L20 atmosphere and 1.4°L43 ocean components. Resolutions of MIROC3h (K-1 model developers, 2004) are higher than MIROC3m and are T106L56 for the atmosphere and eddy-permitting for the ocean (1/4° × 1/6°). Only the horizontal resolution of the atmosphere of MIROC3h is changed to T213 in MIROC4h (Sakamoto et al., 2012). MIROC5 is a medium-resolution model consisting of T85L40 atmosphere and 1.4°L50 ocean components, but with considerably updated physical and dynamical packages (Watanabe et al., 2010). These models have been used to study various scientific issues such as the detection of natural influences on climate changes (e.g., Nozawa et al., 2005; Mori et al, 2014; Watanabe et al., 2014), uncertainty quantification of climate sensitivity (e.g., Shiogama et al., 2012; Kamae et al., 2016), future projections of regional sea-level rises (e.g., Suzuki et al., 2005; Suzuki and Ishii, 2011), and mechanism studies on tropical decadal variability (e.g., Tatebe et al., 2013; Mochizuki et al., 2016).

During the last decade, our efforts have been preferentially devoted to providing science-oriented risk information on climate changes that is beneficial to international, domestic, and municipal communities. For example, so-called event attribution (EA) studies with large ensemble simulations initiated from slightly different conditions have been conducted in order to statistically evaluate influences of the global warming on the occurrence frequencies of observed individual extremes (e.g., Imada et al., 2013; Watanabe et al., 2013; Shiogama et al., 2014). Seasonal-to-decadal climate predictions are also of significant concerns. By initializing prognostic variables in our climate models using observation-based data (Tatebe et al., 2012), significant prediction skills in several specific phenomena, such as the El Niño/Southern Oscillation (ENSO) and the Arctic sea-ice extent on seasonal timescales, the Pacific Decadal Oscillations (PDO; Mantua et al., 1997), the Atlantic Multi-decadal Oscillations (AMO; Schlesinger and Ramankutty, 2004), and the tropical trans-basin interactions between the Pacific and the Atlantic on decadal timescales, are detected (e.g., Mochizuki et al., 2010; Chikamoto et al. 2015; Imada et al., 2015; Ono et al., 2018).

However, while the applicability of MIROC has been extended to a wide range of climate science issues, almost all of the above-mentioned approaches were based on medium-resolution versions of MIROC (MIROC3m and MIROC5), and it is well known that higher-resolution models are capable of better representing the model mean climate and internal climate variability, such as regional extremes, orographic winds, and oceanic western boundary currents/eddies than lower-resolution models (e.g., Shaffrey et al., 2009; Roberts et al., 2009; Sakamoto et al., 2012). Nevertheless, even in high-resolution models, there remain persistent biases associated with, for example, cloud-aerosol-radiative feedback and turbulent vertical mixing of the air in the planetary boundary layer (e.g., Bony and Dufresne, 2005; Bodas-Salcedo et al., 2012; Williams et al., 2013), which are tightly linked with dominant uncertainties in climate projections. Therefore, improvement of physical parameterizations for sub-grid scale processes is essential for better representing observed climatic-mean states and internal climate variability and may result in reducing uncertainty range of climate projections. As well as physical parameterizations, enhanced vertical resolution in both of atmosphere and ocean components, along with a highly accurate tracer advection scheme, have been suggested to have impacts on reproducibility of model-climate and internal climate variations (e.g., Tatebe and Hasumi, 2010; Ineson and Scaife, 2009; Scaife et al., 2012).

Recently, we have developed the sixth version of MIROC, called MIROC6. This newly developed climate model has updated physical parameterizations in all sub-modules. In order to suppress an increase of computational cost, the horizontal resolutions of MIROC6 are not significantly higher than those of MIROC5. The reason is that a larger number of ensemble members are required to realize significant seasonal predictions of, for example, the wintertime Eurasian climate (Murphy et al., 1990; Scaife et al., 2014) because the signal-to-noise ratio is smaller in the mid-latitude atmosphere than in the tropics. Indeed, climate predictions by the older versions of MIROC having at most 10 ensemble members are skillful only in the tropical climate or the mid-latitude oceans. In addition, when evaluating the contributions of internal variations, which will be done in preparation for use in the global stocktake, namely, a five-yearly review of each countries' provisions to climate changes, established by the Paris Agreement in 2015, large ensemble predictions may also be required in decadal-scale predictions. The top of the atmosphere (TOA) in MIROC6 is placed at the 0.004 hPa pressure level which is higher than that of MIROC5 (3 hPa), and the stratospheric vertical resolution has been enhanced in comparison to MIROC5 in order to represent the stratospheric circulations.

Geosci. Model Dev. Discuss., https://doi.org/10.5194/gmd-2018-155
Manuscript under review for journal Geosci. Model Dev.
Discussion started: 16 July 2018

Overall, the reproducibility of the mean climate and internal variability of MIROC6 is better than those of MIROC5, but the model's computational cost is about 3.6 times as large as that of MIROC5. Considering that the computational costs of large ensemble predictions based on high-resolution modeling are still huge on recent computer systems, the use of medium-resolution models with further elaborated parameterizations can still be actively useful in science-oriented climate studies and climate predictions produced for societal needs.

The rest of the present paper is organized as follows. We describe the model configuration, tuning and spin-up procedures in Section 2, while simulated mean-state, internal variability, and climate sensitivity are evaluated in Section 3. Simulation performance of MIROC6 and remaining issues are briefly summarized and discussed in Section 4. Currently, MIROC6 is being used for various simulations designed by the sixth phase of the CMIP (CMIP6; Eyring et al., 2016), which aims to strengthen the scientific basis of the IPCC-AR6. In addition, large ensemble simulations and climate predictions using MIROC6 will be conducted for science-oriented studies in our modeling group, and for societal benefits.

2 Model configurations and spinup procedures

MIROC6 is composed of three sub-models: atmosphere, land, and sea ice-ocean. The atmospheric model is based on the CCSR-NIES atmospheric general circulation model (AGCM; Numaguti et al., 1997). The land surface model is based on Minimal Advanced Treatments of Surface Interaction and Runoff (MATSIRO; Takata et al. 2003), which includes a river routing model of Oki and Sud (2003) based on a kinematic wave flow equation (Ngo-Duc et al., 2007) and a lake module where one-dimensional thermal diffusion and mass conservation are considered. The sea ice-ocean model is based on the CCSR Ocean Component model (COCO; Hasumi, 2006). A coupler system calculates heat and freshwater fluxes between the sub-models in order to ensure that all fluxes are

Geosci. Model Dev. Discuss., https://doi.org/10.5194/gmd-2018-155
Manuscript under review for journal Geosci. Model Dev.
Discussion started: 16 July 2018

conserved within machine precision and then exchanges the fluxes among the sub-models (Suzuki et al., 2009). No flux adjustments are used in MIROC6. In the remaining part of this section, we will provide details of MIROC6 configurations, focusing on updates from MIROC5. Readers may also refer to Table A1 where the updates are briefly summarized.

2.1 Atmospheric component

MIROC6 employs a spectral dynamical core in its AGCM component as in MIROC5. The horizontal resolution is a T85 spectral truncation that is an approximately 1.4° grid interval for both latitude and longitude. The vertical grid coordinate is a hybrid σ-p coordinate (Arakawa and Konor, 1996). The TOA is placed at 0.004 hPa, and there are 81 vertical levels (Fig. 1a). The vertical grid arrangement in MIROC6 is considerably enhanced in comparison to that in MIROC5 (40 levels; 3 hPa) in order that the stratospheric circulations can be represented. A sponge layer that damps wave motions is set at the model top level by increasing Rayleigh friction to prevent extra wave reflection near the TOA. The atmospheric component of MIROC6 has standard physical parameterizations for cumulus convections, radiation transfer, cloud microphysics, turbulence, and gravity wave drag. It also has an aerosol module. These are basically the same as those used in MIROC5, but several updates have been made, as will be detailed below. The parameterizations for cloud micro-physics and planetary boundary layer processes in MIROC6 are the same as in MIROC5.

A cumulus parameterization proposed by Chikira and Sugiyama (2010), which uses an entrainment formulation of Gregory (2001), is adopted in MIROC6 as in MIROC5. This parameterization deals with multiple cloud types including shallow cumulus and deep convective clouds. MIROC5, however, tends to overestimate the low-level cloud amounts over the low-latitude oceans and has a dry bias in the free troposphere. These biases appear to be the result of insufficient vertical mixing of the humid air in the planetary boundary layer and the dry air in the free troposphere is insufficient. To alleviate these biases, an additional parameterization for shallow cumulus convection based on Park and Bretherton (2009) is implemented in MIROC6. Shallow convections associated with the atmospheric instability are calculated by the Chikira and Sugiyama (2010) scheme, and those associated with turbulence in the planetary boundary layer are represented by the Park and Bretherton (2009) scheme. The shallow convective parameterization is a mass flux scheme based on a buoyancy-sorting, entrainment-detrainment single plume model that calculates the vertical transport of liquid water, potential temperature, total water mixing ratio, and horizontal winds in the lower troposphere. The cloud-base mass flux is controlled by turbulent kinetic energy within the sub-cloud layer and convective inhibition. The cloud-base height for shallow cumulus is set between the lifting condensation level and the boundary layer top, which is diagnosed based on the vertical profile of relative humidity. When implementing the parameterization in MIROC6, the following conditions for triggering the shallow convection are specified: 1) The estimated inversion strength (Wood and Bretherton, 2006) is smaller than a tuning parameter, and 2) the convection depth diagnosed by a separate cumulus convection scheme (Chikira and Sugiyama, 2010) is smaller than a tuning parameter.

The Spectral Radiation-Transport Model for Aerosol Species (SPRINTARS; Takemura et al., 2000, 2005, 2009) is used as an aerosol module for MIROC6 to predict the mass mixing ratios of the main tropospheric aerosols which are black carbon, organic matter, sulfate, soil dust, and sea salt, and the precursor gases of sulfate (sulfur dioxide, SO_2, and dimethylsulfide). By coupling the radiation and cloud-precipitation schemes in MIROC, SPRINTARS calculates not only the aerosol transport processes of emission, advection, diffusion, sulfur chemistry, wet deposition, dry deposition, and gravitational settling, but also the aerosol-radiation and aerosol-cloud interactions. There are two primary updates in SPRINTARS of MIROC6 that were not included in MIROC5. One is the treatment of precursor gases of organic matters as prognostic variables. In the previous version, the conversion rates from the precursor gases (e.g., terpene and isoprene) to organic matters are prescribed (Takemura

Geosci. Model Dev. Discuss., https://doi.org/10.5194/gmd-2018-155
Manuscript under review for journal Geosci. Model Dev.
Discussion started: 16 July 2018

et al., 2000), while an explicit simplified scheme for secondary organic matters was introduced from a global chemical climate model (Sudo et al., 2002). The other is a treatment of oceanic primary and secondary organic matters. Emissions of primary organic matters are calculated with wind at a 10-m height, the particle diameter of sea salt aerosols, and chlorophyll-*a* concentration at the ocean surface (Gantt et al., 2011). The oceanic isoprene and monoterpene, which are precursor gases of organic matters, are emitted depending on the photosynthetically active radiation, diffuse attenuation coefficient at 490 nm, and the ocean surface chlorophyll-*a* concentration (Gantt et al., 2009).

The radiative transfer in MIROC6 is calculated by an updated version of the *k*-distribution scheme used in MIROC5 (Sekiguchi and Nakajima 2008). The single scattering parameters have been calculated and tabulated in advance, and liquid, ice, and five aerosol species can be treated in this updated version. Given the significant effect of crystal habit on a particle's optical characteristics (Baran, 2012), the assumption of ice particles habit has been updated from our previous simple assumption of sphere used in MIROC5 to a hexagonal solid column (Yang et al., 2013) in MIROC6. The upper limits of the mode radius of cloud particles have been extended from 32 μm to 0.2 mm for liquids and from 80 μm to 0.5 mm for ice. Therefore, the scheme can now handle the large-sized water particles (e.g., drizzle and rain) that have been shown to have a significant radiative impacts (Waliser et al., 2011). This extended capability is expected to be effective in our future model versions, especially in situations where mass mixing ratios of the large-sized particles are predicted or diagnosed in the cloud microphysics scheme.

Following Hines (1997) and Watanabe et al. (2011), a non-orographic gravity wave parameterization is newly implemented into MIROC6 in order to to represent realistic large-scale circulations and thermal structures in the stratosphere and mesosphere. Together with this parameterization, an orographic gravity wave parameterization of McFarlane (1987) is also adopted as in MIROC5. In both the orographic and non-orographic gravity wave parametrizations, wave source parameters at launch levels are tuned so that the realistic seasonal progress of the middle atmosphere circulations, frequency of sudden stratospheric warmings, and period and amplitude of the equatorial quasi-biennial oscillations (QBOs) can be represented.

2.2 Land surface component

The land surface model is also basically the same as in MIROC5. Energy and water exchanges between land and atmosphere are calculated, considering the physical and physiological effects of vegetation with a single layer canopy, and the thermal and hydrological effects of snow and soil respectively with a three-layers snow and a six-layers soil down to a 14 m depth. Sub-grid fractions of land use and snow cover have also been considered. In addition to the standard package in MIROC5, a few other physical parameterizations are implemented as described below.

A physically-based parameterization of sub-grid snow distribution (SSNOWD; Liston, 2004; Nitta et al., 2014) replaces the simple functional approach of snow water equivalent in calculating sub-grid snow fractions in MIROC5. In SSNOWD, the snow cover fraction is formulated for accumulation and ablation seasons separately. For the ablation season, the snow cover fraction decreases based on the sub-grid distribution of the snow water equivalent. A lognormal distribution function is assumed and the coefficient of variation category is diagnosed from the standard deviation of the sub-grid topography, coldness index, and vegetation type that is a proxy of surface winds. While the cold degree month was adopted for coldness in the original SSNOWD, we decided instead to introduce the annually averaged temperature over the latest 30 years using the time-relaxation method of Krinner et al. (2005), in which the timescale parameter is set to 16 years. The temperature threshold for a category diagnosis is set to 0°C and 10°C. In addition, a scheme representing a snow-fed wetland that takes into consideration sub-grid terrain complexity (Nitta et al., 2017) is incorporated. The river routing model and lake module are the same as those used in MIROC5, but the river network map is updated to keep the consistency to the new land-sea mask (Yamazaki et al., 2009).

2.3 Ocean and sea-ice component

The ocean component of MIROC6 is basically the same as that used in MIROC5, but several updates are implemented as described below. The warped bipolar horizontal coordinate system in MIROC5 has been replaced by the tripolar coordinate system proposed by Murray (1996). Two singular points in the bipolar region to the north of about 63°N are placed at (63°N, 60°E) in Canada and (63°N, 120°W) in Siberia (Fig. 2). In the spherical coordinate portion to the south of 63°N, the longitudinal grid spacing is 1° and the meridional grid spacing varies from about 0.5° near the equator to 1° in the mid-latitudes. In the central Arctic Ocean where the bipole coordinate system is applied, the grid spacings are about 60 km in zonal and 33 km in meridional, respectively. There are 62 vertical levels in a hybrid σ-z coordinate system. The horizontal grid spacing in MIROC5 is nominally 1.4°, except for the equatorial region and there are 49 vertical levels. The resolutions in MIROC6 are higher than in MIROC5. In particular, 31 (23) of the 62 (49) vertical layers in MIROC6 (MIROC5) are within the upper 500 m depth (Fig. 1b). The increased vertical layers in MIROC6 have been adopted in order to better represent the equatorial thermocline and observed complex hydrography in the Arctic Ocean. An increase in computational costs of the ocean component due to higher resolutions in MIROC6 is suppressed by implementing a time-staggered scheme for the tracer and baroclinic momentum equations (Griffies et al., 2005).

The tracer advection scheme (Prather, 1986), the surface mixed layer parameterization (Noh and Kim, 1999), and the parameterization for eddy isopycnal diffusion (Gent et al., 1995) used in MIROC6 are the same as those used in MIROC5. Also as in MIROC5, the bottom boundary layer parameterization of Nakano and Suginohara (2002) is introduced south (north) of 54°S (49°N) for representing the down-sloping flow of dense waters. The constant parameters used in the above-mentioned parameterizations are determined in the same manner as that of MIROC5, except for the Arctic region. An empirical profile of background vertical diffusivity, which is proposed in Tsujino et al. (2000), is modified above the 50 m depth to the north of 65°N. It is 1.0×10^{-6} m^2 s^{-1} in the uppermost 29 m and gradually increases to 1.0×10^{-5} m^2 s^{-1} at the 50 m depth. Additionally, the turbulent mixing process in the surface mixed layer is changed so that there is no surface wave breaking and no resultant near-surface mixing in regions covered by sea ice. The combination of the weak background vertical diffusivity and suppression of turbulent mixing under the sea-ice contributes to better representations of the surface stratification in the Arctic Ocean with little impact on the rest of the global oceans (Komuro, 2014).

The sea-ice component in MIROC6 is almost the same as in MIROC5. A brief description, along with some major parameters, is given here. Readers may refer to Komuro et al. (2012) and Komuro and Suzuki (2013) for further details. A subgrid-scale sea-ice thickness distribution is incorporated by following Bitz et al. (2001). There are five ice categories (plus one additional category for open water), and the lower bounds of the ice thickness for these categories are set to 0.3, 0.6, 1, 2.5, and 5 m. The momentum equation for sea-ice dynamics is solved using elastic-viscous-plastic rheology (Hunke and Dukowicz, 1997). The strength of the ice per unit thickness and concentration is set at 2.0×10^4 N m^{-2}, and the ice–ocean drag coefficient is set to 0.02. The surface albedo for bare ice surface is 0.85 (0.65) for the visible (infrared) radiation. The surface albedo in snow-covered areas is 0.95 (0.80) when the surface temperature is lower than -5ºC for the visible (infrared) radiation, and it is 0.85 (0.65) when the temperature is 0ºC. Note that the albedo changes linearly between -5ºC and 0ºC. These parameter values listed here are the same as those listed in MIROC5.

2.4 Boundary conditions

Geosci. Model Dev. Discuss., https://doi.org/10.5194/gmd-2018-155
Manuscript under review for journal Geosci. Model Dev.
Discussion started: 16 July 2018

Geoscientific Model Development Discussions
Open Access

A set of external forcing data recommended by the CMIP6 protocol are used. The historical solar irradiance spectra, greenhouse gas concentrations, anthropogenic aerosol emissions, and biomass burning emissions are given by Matthes et al. (2017), Meinshausen et al. (2017), Hoesly et al. (2018), and van Marle et al. (2017), respectively. The concentrations of greenhouse gases averaged globally and annually are given to MIROC6. Stratospheric aerosols due to volcanic eruptions, which are provided by Thomason et al. (2016), are taken into account as extinction coefficients for each radiation band. Three-dimensional atmospheric concentrations of historical ozone (O_3) are produced by the Chemistry-Climate Model Initiative (Hegglin et al., in preparation; the data are available at http://blogs.reading.ac.uk/ccmi/forcing-databases-in-support-of-cmip6/). Three dimensional concentrations of the OH radical, hydrogen peroxide (H_2O_2) and Nitrate (NO_3) are precalculated by a chemical atmospheric model of Sudo et al. (2002). As precursors of secondary organic aerosol, emission data of terpenes and isoprene provided by the Global Emissions Inventory Activity (Guenther et al., 1995) are normally used, although simulated emissions from the land ecosystem model of Ito and Inatmoni (2012) are also used alternatively.

For specifying the soil types and area fractions of natural vegetation and crop-land on grids of the land-surface component, the harmonized land-use dataset (Hurtt et al., in prep.), Center for Sustainability and the Global Environment global potential vegetation dataset (Ramankutty and Foley, 1999), and the dataset provided by the International Satellite Land Surface Climatology Project Initiative I (Sellers et al., 1996) are used. This datasets are also used in prescribing background reflectance at the land surface. Leaf-area index data are prepared based on the Moderate Resolution Imaging Spectroradiometer Leaf-area index products of Myneni et al. (2002).

The forcing dataset used for the preindustrial control simulation is basically composed of the data for the year 1850, which are included in the above-mentioned historical dataset. The stratospheric aerosols and solar irradiance in the preindustrial simulation are given as monthly

Geosci. Model Dev. Discuss., https://doi.org/10.5194/gmd-2018-155
Manuscript under review for journal Geosci. Model Dev.
Discussion started: 16 July 2018

climatology in 1850 – 2014 and in 1850 – 1873, respectively. The total solar irradiance is about 1361 Wm^{-2}, and the global-mean concentrations of CO_2, methan (CH_4), and nitrous oxide (N_2O) are 284.32 ppm, 808.25 ppb, and 273.02 ppb, respectively.

2.5 Spin-up and tuning procedures

Firstly, the stand-alone ocean component of MIROC6, which includes the sea-ice processes, is integrated from the initial motionless state with the observed temperature and salinity distribution of the Polar Science Center hydrographic climatology (Steele et al., 2001). The ocean component is spun-up for 1000 years by the monthly climatological surface fluxes of Röske (2006). An acceleration method of Bryan (1984) is used in the spin-up stage in order to obtain a thermally and dynamically quasi-steady state. After the spin-up, additional integration for 200 years is performed without the acceleration method. By analyzing the last 50-yr-long data from the stand-alone ocean component, the monthly climatology of typical variables (e.g., zonal-mean temperature and salinity in several basins, volume transports across major straits and archipelagos, meridional overturning circulations, and sea-ice distributions) are compared with observations. Once the configuration of the ocean component is frozen, the land-sea distribution and land-sea area ratios on the model grids of the atmospheric and land surface components are determined, after which the atmospheric and the land surface components are coupled with the ocean component. An initial condition of the ocean component in MIROC6 is given by the stand-alone ocean experiment, and those of the atmosphere and land are taken from an arbitrary year of the pre-industrial control run of MIROC5.

After coupling the sub-models, climate model tuning is done under the pre-industrial boundary conditions. Conventionally, the climate models of our modeling community are retuned in coupled modes after stand-alone sub-model tuning. This is because reproducibility is not necessarily guaranteed in climate models with the same parameters determined in stand-alone sub-model tuning, which is particularly the case in the tropical climate. In our tuning procedures described below, many of the 10-yr-long climate model runs are conducted with different parameter values. There are numerous parameters associated with physical parameterizations, whose upper/lower bounds are constrained by empirical or physical reasoning. The main parameters used in our tuning procedures are stated in the next paragraph and are chosen primarily referring to Shiogama et al. (2012), in which the uncertainty of the climate sensitivity in MIROC5 is extensively measured using a perturbed parameter ensemble set. The impact of parameter tuning on the present climate is also discussed by Ogura et al (2017), focusing on the TOA radiation and clouds. Any objective and optimal methods for parameter tuning are not used in our modeling group and the tuning procedures are like those in other climate modeling groups as summarized in Hourdin et al. (2017).

In the first model tuning step, climatology, seasonal progression, and internal climate variability in the tropical coupled system are tuned in order that departures from observations or reanalysis datasets are reduced. Here, it should be noted that representation of the tropical system in MIROC6 is sensitive to the parameters for cumulus convection and planetary boundary layer processes. Next, the wintertime mid-latitude westerly jets and the stationary waves in the troposphere are tuned using the parameters of the orographic gravity wave drag and the hyper diffusion of momentum. The parameters of the hyper diffusion and the non-orographic gravity wave drag are also used when tuning stratospheric circulations of the polar vortex and QBO. Finally, the radiation budget at the TOA is tuned, primarily using the parameters for the auto-conversion process so that excess downward radiation can be minimized and maintained closer to 0.0 Wm^{-2}. The surface albedos for bare sea-ice and snow-covered sea-ice are set to higher values than in observations (see Section 2.3) in order to avoid underestimating of the summertime sea-ice extent in the Arctic Ocean due to excess downward shortwave radiation in this region. In addition, parameter tuning for cooling effects due to interactions between anthropogenic aerosol emissions and cloud-radiative processes are done. In order that the cooling effects can be closer to the estimate of -0.9 Wm^{-2} (IPCC, 2013; negative value indicates cooling) with an uncertainty range of -1.9 to -0.1 Wm^{-2}, parameters of cloud microphysics and the aerosol transport module, such as timescale for cloud droplet nucleation, in-cloud properties of aerosol removal by precipitation, and minimum threshold of number concentration of cloud droplets, are perturbed. To determine a suitable parameter set, several pairs of a present-day run under the anthropogenic aerosol emissions at the year 2000 and a pre-industrial run are conducted. A pair of the present and preindustrial runs has exactly the same parameters, and differences of tropospheric radiations between two runs are considered as anthropogenic cooling effects.

After fixing the model parameters, the climate model is spun-up for 2000 years. During the first several hundred years, waters contained in the land surface are drained to the ocean via river runoff, which leads to a temporal weakening of the meridional overturning circulations in the ocean and a rising of the global-mean sea level. After the global hydrological cycle reaches to an equilibrium state, the strengths of the meridional overturning circulations recover and keep quasi steady state. The above-mentioned processes spend about 1000 years, after which an additional 1000-yr-long integration is performed in order to obtain a thermally and dynamically quasi-steady ocean state.

Figure 3 shows the time series of the global-mean quantities after the spin-up. The labeled year in Fig. 3 indicates the elapsed year after the spin-up duration of 2000 years. The global-mean surface air temperature (SAT) and the radiation budget at the TOA show no significant drifts, thereby indicating that they are in a quasi-steady state. Linear trends of the global-mean SAT and the radiation budget are 9.5×10^{-3} K/100yr and 2.1×10^{-3} Wm^{-2}/100yr, respectively. The trend of the SAT is much smaller than the observed value of about 0.62 K/100 yr in the twentieth century. While the global-mean sea surface temperature (SST) is in a quasi-steady state (linear trend of 7.0×10^{-3} K/100 yr), the global-mean ocean temperature shows a larger trend of 6.8×10^{-3} K/100 yr in the first 500 years than that of 1.3×10^{-3} K/100 yr in the later period. The larger trend in the global-mean ocean temperature suggests that the deep ocean continues to warm slightly. In the later sections, the 200-yr-long data between the 500-th and 699-th years are analyzed.

3 Results of pre-industrial simulation

Representations of climatic-mean field and internal climate variability in MIROC6 are evaluated in comparison with MIROC5 and observations. The 200-yr-long data of the preindustrial control simulation by MIROC5 are used. The observations and reanalysis datasets used in the comparison are listed in Table 1.

Here, the model climatology in the pre-industrial simulations is compared with observations in the recent decades. Because observations are obtained concurrently with the progress of the global-warming due to increasing anthropogenic radiative forcing, the model climate under the pre-industrial conditions may not be adequate for use when making comparisons with recent observations. However, the root-mean-squared (RMS) errors of typical variables (e.g., the global-mean SAT) in the climate models with respect to observations are much larger than the RMS differences between the model climatology in the pre-industrial simulation and those in the last 30-yr-long period in the historical simulations. Therefore, the era differences where climatology is defined are not significant concern in comparisons among the climate models and observations.

3.1 Climatology

3.1.1 Atmosphere and Land-surface

First, model systematic biases in radiations at the TOA are evaluated because they reflect model deficiencies in cloud-radiative processes that contribute to a large degree of uncertainty in climate modelling. Figure 4 shows annual-mean biases in radiative fluxes at the TOA in MIROC6 and MIROC5 with respect to the recent Clouds and the Earth's Radiant Energy System (CERES) estimate

Geosci. Model Dev. Discuss., https://doi.org/10.5194/gmd-2018-155
Manuscript under review for journal Geosci. Model Dev.
Discussion started: 16 July 2018

(Loeb et al., 2009; the data are available at https://ceres.larc.nasa.gov/). At the top-right of each panel, a global-mean (GM) value and a root-mean-squared error (RMSE) with respect to observations are written. Because the modeled and observed global-mean values are not considered when calculating the RMSE, the RMSE reflects model errors in spatial distribution.

Persistent overestimates in the net and outgoing shortwave radiative fluxes (hereafter, NET and OSR, respectively) over low-latitude oceans in MIROC5 are significantly reduced in MIROC6. As described in Ogura et al. (2017), since parameter tuning cannot eliminate the above-mentioned excess upward radiations, it is suggested that implementing a shallow convective parameterization is required in order to reduce the biases. Figure 5 shows annual-mean moistening rates associated with deep and shallow convections at the 850 hPa pressure level in MIROC6, which has a shallow convective parameterization based on Park and Bretherton (2009). Moistening due to shallow convections occurs mainly over the low-latitude oceans, especially the eastern subtropical Pacific and the western Atlantic and Indian oceans. These active regions of shallow convections occur separately from regions with active deep convections in the western tropical Pacific and the Inter-Tropical Convergence Zone (ITCZ). The clear separation of the two convection types is consistent with satellite-based observations (Williams and Tselioudis, 2007). Owing to the shallow convective process that mixes the humid air in the planetary boundary layer with the dry air in the free troposphere, low-level cloud cover over the low-latitude oceans is better represented in MIROC6 than in MIROC5. Figure 6 shows annual-mean biases in cloud covers with respect to the International Satellite Cloud Climatology Project (ISCCP; Rosso et al., 1996; Zhang et al., 2004; the data are available at https://isccp.giss.nasa.gov/). Overestimate of low-level cloud cover over the low-latitude oceans in MIROC5 (Fig. 6b) is apparently reduced in MIROC6 (Fig. 6a), which results in the smaller biases in NET and OSR biases (Fig. 4). RMS error in low-level cloud cover in MIROC6 is 9% lower than that in MIROC5.

Geosci. Model Dev. Discuss., https://doi.org/10.5194/gmd-2018-155
Manuscript under review for journal Geosci. Model Dev.
Discussion started: 16 July 2018

OSR in the mid-latitudes are also better represented in MIROC6 than in MIROC5. Zonally distributed downward OSR bias in MIROC5 is reduced or becomes a relatively small upward bias in MIROC6 (Figs. 4cd). This difference in the OSR bias is commonly found in both hemispheres. Cloud covers at middle and high levels are larger in MIROC6 over the subarctic North Pacific, North Atlantic, and the Southern Ocean (Figs. 6c-f), while low-level cloud cover over the same regions is smaller in MIROC6 than in MIROC5 over the same regions (Figs. 6ab). The smaller low-level cloud cover in MIROC6 is inconsistent with the larger upward OSR bias in MIROC6. The wintertime mid-latitude westerlies are stronger and are located more poleward in MIROC6 than in MIROC5. Correspondingly, activity of sub-weekly disturbances in the mid-latitudes is strengthened in MIROC6 (details are described later). These differences in the mid-latitude atmospheric circulations between MIROC6 and MIROC5 lead to an enhanced poleward moist air transport from the subtropics to the subarctic region, which could result in an increase in the mid- and high-level cloud covers in MIROC6, as reported in previous modeling studies (e.g., Bodas-Salcedo et al., 2012; Williams et al., 2013). Consequently, the downward OSR bias in the mid-latitudes is smaller in MIROC6 than in MIROC5. In polar regions, both biases in OSR and NET remain the same as in MIROC5.

Systematic bias in the outgoing longwave radiative flux (hereafter, OLR) is worse in MIROC6 than in MIROC5 because MIROC6 tends to underestimate OLR over almost the entire global domain, except for Antarctica (Figs. 4ef). The global-mean of the high-level cloud cover in MIROC6 is larger than in MIROC5 by 0.04 (Figs. 6ef), which is consistent with the smaller OLR in MIROC6. The increased moisture transport due to the strengthening of the westerlies and sub-weekly disturbances can partly explain the increase in the mid-latitude high-level clouds in MIROC6, but high-level cloud cover is also larger in the low-latitudes. Hirota et al. (2018) reported that moistening of the free troposphere due to shallow convections creates favorable conditions for atmospheric instabilities that leads to the resultant activation of deep convections in the low-latitudes. Such

Geosci. Model Dev. Discuss., https://doi.org/10.5194/gmd-2018-155
Manuscript under review for journal Geosci. Model Dev.
Discussion started: 16 July 2018

processes may contribute to the inferior representation of OLR in MIROC6.

Next, we will discuss on the global budget of the radiative fluxes and the RMS errors between models and observations. Note that only deviations from the global means are considered when calculating RMS errors. As written on the upper right of panels in Fig. 4ab, the global-mean (RMS errors) NETs are -1.11 (12.7) Wm^{-2} in MIROC6 and -0.98 (15.9) Wm^{-2} in MIROC5, respectively, and these values are consistent with the observed value of -0.81 Wm^{-2}. However, if NET is divided into OSR and OLR, so-called error compensation becomes apparent. The global means of OSR (OLR) are -231.3 (230.2) Wm^{-2} in MIROC6 and -237.6 (236.6) Wm^{-2} in MIROC5, respectively (Figs. 4c-f). The observed global-means of OSR and OLR are -240.5 Wm^{-2} and 239.7 Wm^{-2}. Biases in the global-mean OSR (OLR) with respect to observations are 9.2 (-9.5) Wm^{-2} in MIROC6 and 2.9 (3.1) Wm^{-2} in MIROC5, respectively. Thus, the global-mean OSR and OLR in MIROC6 are worse than those in MIROC5. Further division of OSR and OLR into cloud-radiative forcing and clear-sky shortwave (longwave) radiative components shows that shortwave cloud-radiative forcing is dominant on the biases in radiative fluxes. The biases in the global-mean shortwave (longwave) cloud-radiative forcing with respect to observations are 12.0 (6.7) Wm^{-2} in MIROC6 and -4.0 (-0.2) Wm^{-2} in MIROC5, respectively.

The global radiation budget in MIROC6 is inferior to that in MIROC5, while reproducibility of climatic means of typical model variables, other than radiative fluxes, and internal variations are better simulated in MIROC5 (details are shown later). As described in Section 2.5, the intensive tuning by perturbing model parameters is done focusing on reproducibility of climatic means, internal variations, and radiative forcing due to anthropogenic aerosols. During this procedure, the global radiation budget is traded-off. On the other hand, RMS errors in NET, OSR, and OLR are 12.7, 16.2, and 6.3 Wm^{-2} in MIROC6 and 15.9, 18.9, and 6.8 Wm^{-2} in MIROC5, respectively, thereby indicating that the errors in MIROC6 have been reduced by 7% to 20 %. This is also the case for shortwave and longwave cloud radiative forcings, where the corresponding errors have been reduced by 17% and 13 %, respectively. Taken toghther, these results show that the spatial patterns of the radiative fluxes are better simulated in MIROC6 than in MIROC5.

The improvement in spatial radiation patterns, especially in low-latitude OSR, is explained primarily by the implementation of shallow convective processes, which results in a moister free troposphere in MIROC6 than in MIROC5. Figures 7ab show zonal-mean biases in annual-mean specific humidity with respect to the European Centre for Medium-Range Weather Forecast interim reanalysis (ERA-I; Dee et al., 2011; the data are available at https://www.ecmwf.int/en/forecasts/datasets/archive-datasets/reanalysis-datasets/era-interim). Dry bias in 30ºS–30ºN, which occurs persistently in MIROC5, are largely reduced in MIROC6 owing to vertical mixing at the interface of the planetary boundary layer and the free troposphere. On the other hand, moist bias below the 600 hPa pressure level in the mid-latitudes is somewhat worse in MIROC6 than in MIROC5. Shallow convections also contribute to the improvement of precipitations in the low latitudes. Figure 8 shows global maps for climatological precipitation in boreal winter (December–February) and summer (June–August). The second version of the Global Precipitation Climatology Project (GPCP; the data are available at https://precip.gsfc.nasa.gov/) Monthly Precipitation Analysis (Adler et al., 2003) is used for the observations. While MIROC5 suffers from underestimate of summertime precipitation over the western tropical Pacific, the underestimate is largely reduced in MIROC6 (Figs. 8df). The increase of precipitations is associated with deep convections because the moister free troposphere in MIROC6 is more favorable for the occurrence of deep convections (Hirota et al., 2018).

Zonal-mean biases in annual-mean air temperature and zonal wind velocity are also better represented in MIROC6 than in MIROC5 (Figs. 7c-f). The remarkable upper stratospheric warm bias in 50ºS–50ºN in MIROC5 is significantly reduced in MIROC6. The TOA in MIROC6 is located at the

Geosci. Model Dev. Discuss., https://doi.org/10.5194/gmd-2018-155
Manuscript under review for journal Geosci. Model Dev.
Discussion started: 16 July 2018

0.004 hPa pressure level and there are 42 vertical layers above the 50 hPa pressure level, while the TOA of MIROC5 is placed at the 3 hPa pressure level. As a result, there are significant differences in stratospheric circulations between the models. As shown in the annual-mean mass stream function with $\log_{10}$ vertical scale (Fig. 9), an upward wind from the tropopause to the stratopause is apparent in low-latitudes of MIROC6. This upward wind transports the cold air in the temperature minimum around the tropopause in 30ºS–30ºN, which reduces the warm bias in the stratosphere. Correspondingly, the stratospheric westerly bias in low latitudes of MIROC5 is also considerably alleviated in MIROC6. Note that the atmospheric O_3 concentration data used in MIROC5 is different from those in MIROC6, and the concentration in the stratosphere is higher than the data used in MIROC6. About 25% of the above-mentioned reduction in the stratospheric warm biases is explained by the smaller absorption of longwave radiation by O_3.

The zonal-means of the air temperature and zonal wind in MIROC6 are also better simulated in the mid- and high latitudes. A pair of easterly and westerly biases in MIROC5, which is in the troposphere of the Northern Hemisphere, is associated with a weaker mid-latitude westerly jet and its southward shift with respect to observations. The pair of the biases is reduced in MIROC6, thereby suggesting that a strengthening and northward shift of the westerly jet occurs in MIROC6. Indeed, as shown in the upper panels of Fig. 10, the meridional contrast of high and low biases in the 500 hPa pressure level (Z500) along the wintertime westerly jet is weaker in MIROC6 than in MIROC5. The latitudes with the maximal meridional gradient of Z500 are located further northward in MIROC6 than in MIROC5, especially over the North Atlantic. Correspondingly, wintertime storm track activity (STA), which is defined as an 8-day-high-pass-filtered eddy meridional temperature flux at the 850 hPa pressure level, is stronger over the North Pacific and Atlantic in MIROC6 than in MIROC5 (see upper panels of Fig. 11) and is accompanied by an associated increase in precipitation (Figs. 8ce). In the stratosphere above the 10 hPa pressure level, the polar night jet is reasonably captured in MIROC6, although the westerly is somewhat overestimated in 30ºN–60ºN. Also, in the Southern Hemisphere, representation of the tropospheric westerly and the polar night jets are better in MIROC6 than in MIROC5, and the easterly bias centered at 60ºS in the troposphere is clearly reduced in MIROC6. Although causality is unclear, the warm air temperature bias above the tropopause to the south of 60ºS is smaller in MIROC6 than in MIROC5.

The enhanced wintertime STA in MIROC6 leads to a strengthening of the Ferrel circulation in the Northern Hemisphere and a broadening of its meridional width. As shown in Fig. 9, the northern edge of the Ferrel cell is located further northward in MIROC6 than in MIROC5. Because the Ferrel cell is a thermally indirect circulation driven primarily by eddy temperature and momentum fluxes, the stronger STA in MIROC6 possibly causes the Ferrel cell differences between the two models. Associated with the northward extension of the Ferrel cell, the upward wind between the Ferrel cell and the polar cell centered at 65ºN is stronger in MIROC6 than in MIROC5 and the meridional width of the polar cell is smaller. Also, in the Southern Hemisphere, the upward wind around 60ºS at the southern edge of the Ferrel cell is stronger in MIROC6 than in MIROC5. Correspondingly, high sea level pressure (SLP) biases in polar region in MIROC5 are significantly reduced in MIROC6 (figures are omitted) and RMS errors with respect to observations (ERA-I) are decreased by 30 %. Meanwhile, in the stratosphere, anti-clockwise (clockwise) circulations to the north (south) of 50ºN (S) are stronger and extends further upward in MIROC6 than in MIROC5. These circulations seem to continue from the troposphere into the stratosphere, thereby implying that more active troposphere-stratosphere interactions exist in MIROC6. Further details will be described later, focusing on the occurrence of the sudden stratospheric warmings.

Parameterizations of SSNOWD (Liston, 2004; Nitta et al., 2014) and a wetland due to snow-melting water have been newly implemented into MIROC6 (Nitta et al., 2017). In comparison of MIROC6 with MIROC5, it can be seen that the former parameterization brings about remarkable

Geosci. Model Dev. Discuss., https://doi.org/10.5194/gmd-2018-155
Manuscript under review for journal Geosci. Model Dev.
Discussion started: 16 July 2018

Geoscientific Model Development Discussions
Open Access

improvement in the Northern Hemisphere snow cover fractions (Fig. 12). Compared with observations of the Northern Hemisphere EASE-Grid 2.0 (Brodzik and Armstrong, 2013; the data are available at https://nsidc.org/data/ease/), the distribution of the snow cover fractions is more realistic in MIROC6 than MIROC5, especially where and when the snow water equivalent is relatively small (e.g., mid- and high latitudes in November, over Siberia in February). This is because the newly implemented SSNOWD represents hysteresis in the snow water equivalent-snow cover fraction relationship in both the accumulation and ablation seasons. MIROC6 underestimates the snow cover fraction in the partially snow-covered regions and overestimates it on the Tibetan plateau and in some parts of China. We note that meteorological (e.g., precipitation or temperature) phenomena might affect these biases, but further investigation will be necessary to identify their causes. Nevertheless, in spite of those discrepancies, it can be said that the seasonal changes of the snow cover fraction are better simulated in MIROC6 than in MIROC5 (Fig. 12j).

3.1.2 Ocean

Next, we evaluate the climatological fields of the ocean hydrographic structure, meridional overturning circulations (MOCs), and sea-ice distribution. The zonal-mean potential temperature and salinity are displayed in Figs. 13 and 14, respectively. Both MIROC6 and MIROC5 capture the general features of the observed climatological hydrography (ProjD; Ishii et al., 2003). In the deep and bottom layers to the south of 60ºS, into which cold and dense water forms due to intense surface cooling around Antarctica sinks, the potential temperatures in the two models are warmer than observations (Figs. 13a-c and 14a-c), as are the potential temperatures in northern high latitudes of the Atlantic sector (Figs. 13a-c). By horizontal advection of the warm temperature biases associated with the Pacific and Atlantic MOCs, the model temperatures in deep layers other than polar regions are also warmer than in observations. In general, the deep water distribution in MIROC6 remains the same as

Geosci. Model Dev. Discuss., https://doi.org/10.5194/gmd-2018-155
Manuscript under review for journal Geosci. Model Dev.
Discussion started: 16 July 2018

in MIROC5.

Meanwhile, the northward intrusion of Antarctic Intermediate Water in the Southern Hemisphere around the 1000 m depth is better simulated in MIROC6 than in MIROC5, especially in the Pacific sector (Figs. 13a-c). In the Arctic Ocean, the halocline above the upper 500 m depth is sharper and more realistic in MIROC6 than in MIROC5 because, as described in Section 2.3, there are many more vertical levels in the surface and subsurface layers of MIROC6. In addition, vertical diffusivity in the Arctic Ocean is set to smaller values in MIROC6 than in MIROC5, and the turbulent kinetic energy input induced by surface wave breaking, as a function of the sea-ice concentration in each grid cell, is reduced in MIROC6, as shown in Komuro (2014). These differences in the ocean model configuration are considered likely to contribute to the improved oceanic structures in the surface and intermediate layers. In the North Pacific, the southward intrusion of North Pacific Intermediate Water (NPIW) around the 1000 m depth retreats northward in MIROC6. Strong tide-induced vertical mixing of sea water is observed along the Kuril Islands (e.g., Katsumata et al., 2004). The locally enhanced tide-induced mixing is known to reinforce the southward intrusion of the Oyashio and associated water mass transport from the subarctic to subtropical North Pacific, and to feed the salinity minimum of NPIW (Nakamura et al., 2004; Tatebe and Yasuda, 2004). Hence, in situations where enhanced tidal mixing is considered, NPIW reproducibility is better in MIROC5 than in MIROC6. Because we encountered significant uncertainty in implementing the tidal mixing, and we decided to quit implementing it in developing phase of MIROC6, at the expense of NPIW reproducibility.

The annual-mean potential temperature and zonal currents along the equator in MIROC6 are better simulated in MIROC6 than in MIROC5 (Fig. 15). Relatively cold water below the equatorial thermocline is risen in MIROC6, especially in the eastern tropical Pacific, which leads to a strengthening of the vertical temperature gradient across the thermocline. The eastward speed of the

Equatorial Undercurrent in MIROC6 is over 80 cm s^{-1}, and is closer to the products of Simple Ocean Data Assimilation (SODA; Carton and Giese, 2008; the data are available at http://www.atmos.umd.edu/~lchen/SODA3.3_Description.html) than in MIROC5. These improvements are mainly attributed to the higher vertical resolution of MIROC6 in the surface and subsurface layers. However, the thermocline depths in the western tropical Pacific are still larger in the models than in observations. This is due to the stronger trade winds in the models, which is a deficiency that also appears in stand-alone AGCM experiments. Hence, better representation of cloud physics in the models may be required in the future.

Figure 16 displays annual-mean Atlantic and Pacific MOCs. In the Atlantic, two deep circulation cells associated with North Atlantic Deep Water (NADW; upper cell) and Antarctic Bottom Water (AABW, lower cell) are found in both of the models. NADW transport across 26.5ºN is 17.2 (17.6) Sv (1 Sv = 10^6 m^3 s^{-1}) in MIROC6 (MIROC5). These values are consistent with the observational estimate of 17.2 Sv (McCarthy et al., 2015). RMS amplitudes of NADW transport are about 0.9 Sv in MIROC6 and 1.1 Sv in MIROC5 on longer-than-interannual timescales, respectively. These are smaller than the observed amplitude of 1.6 Sv in 2005–2014. Because observations include the weakening trend of the Atlantic MOC due to the global warming, they can be larger than the model variability under the preindustrial conditions. In the Pacific Ocean, both the models have the deep circulation associated with Circumpolar Deep Water (CDW), but the northward transport of CDW across 10ºS is 8.6 Sv in MIROC6, which is slightly larger than 7.5 Sv of MIROC5. Although these models values are somewhat smaller than observations, they are within the uncertainty range of observations (Talley et al., 2003; Kawabe and Fujio, 2010).

Northern Hemisphere sea-ice concentrations are shown in Fig. 17. Here, it can be seen that both the March and September sea-ice distributions in MIROC6 resemble to the satellite-based observation (SSM/I; Cavarieli et al., 1991; the data are available at https://nsidc.org/). In general, the spatial patterns of the models resemble the observations. Sea-ice areas in March (September) are 12.4 (6.1), 13.0 (6.9), and 14.9 (5.7) Million km^2 in MIROC6, MIROC5, and observations, respectively. The model estimates are smaller (larger) in March (September) than in observations. The underestimate in March is still found in MIROC6 and is attributed to the underestimate of sea-ice area in the Sea of Okhotsk and the Gulf of St. Lawrence, even though the sea-ice area in the former region is better simulated in MIROC6 than in MIROC5. Meanwhile, the eastward retreat of the sea-ice in the Barents Sea is better represented in MIROC6 than in MIROC5. The overestimates in September in the models are due to that the model climatology is defined under the pre-industrial conditions while observations are taken in present-day conditions, where a rapid decreasing trend of summertime sea-ice area (including a few events of drastic decreases) is on-going (e.g., Comiso et al., 2008). On the other hand, the modeled sea-ice areas in the Southern Ocean are unrealistically smaller than in observations. Southern Hemisphere sea-ice areas in March (September) are 0.1 (3.4), 0.2 (5.2), and 5.0 (18.4) Million km^2 in MIROC6, MIROC5, and observations, respectively. Since there are no remarkable differences between the two models, the spatial maps for the sea-ice area in the southern hemisphere are omitted.

Figure 18 shows the global maps of annual-mean sea level height. Although overall oceanic gyre structures in MIROC6 remain generally the same as in MIROC5, there are a few improvements in the North Pacific and the North Atlantic. The mid-latitude westerly in MIROC6 is stronger and is shifted further northward than in MIROC5 (Fig. 10), which results in the strengthening of the subtropical gyres, northward shifts of the western boundary currents, and their extensions. In particular, the current speed of the Gulf Stream and the North Atlantic Current are faster in MIROC6 than in MIROC5, and the contours emanating from the North Atlantic reach the Barents Sea in MIROC6. A corresponding increase in warm water transport from the North Atlantic to the Barents Sea leads to sea-ice melting and an eastward retreat of the wintertime sea-ice there in MIROC6 (Figs.

17a-c). A remarkable improvement in MIROC6 is also found in the Subtropical Countercurrent (STCC) in the North Pacific along 20ºN. As reported in Kubokawa and Inui (1999), the low potential vorticity water associated with a wintertime mixed layer deepening in the western boundary current region is transported southward in the subsurface layer and it pushes up isopycnal surfaces around 25ºN. Thus, the eastward-flowing STCC is induced around 25ºN. Although both of the models show the wintertime mixed layer deepening, the ocean stratification along 160ºE is weaker in MIROC6 than in MIROC5 (not shown). This suggests that the isopycnal advection of low potential vorticity water in MIROC6 is more realistic than in MIROC5.

3.1.3 Discussions on model climatological biases

We have evaluated the simulated climatology in MIROC6 in comparison with MIROC5 and observations. The model climatology in MIROC6 shows certain improvements in simulating radiations, atmospheric and oceanic circulations, and land surface variables. In Fig. 19, we display the model biases in annual-mean SAT and SST (Fig. 19) because these are typical variables that reflect errors in individual processes in the climate system. The global-mean of SAT (SST) is 15.2 (18.1) ºC in MIROC6, 14.6 (18.0) ºC in MIROC5, and 14.4 (18.1) ºC in observations. The modeled global-mean SATs and SSTs are generally consistent with observations. Here, it should be noted that while the spatial patterns of the SAT and SST biases in MIROC6 resemble those in MIROC5, there are several improvements. For example, cold SAT bias in MIROC5 extending from the Barents Sea to Eurasia is significantly smaller in MIROC6, possibly owing to the increase in warm water transport by the North Atlantic Current and the resultant eastward retreat of the sea ice in the Barents Sea (Figs. 17 and 18). Warm SAT and SST biases along the west coast of the North America are smaller in MIROC6 than in MIROC5, thereby suggesting that the strengthening of the mid-latitude westerly jet (Fig. 10) and the associated strengthening of the Aleutian low lead to increase in southward transport of relatively cold

Geosci. Model Dev. Discuss., https://doi.org/10.5194/gmd-2018-155
Manuscript under review for journal Geosci. Model Dev.
Discussion started: 16 July 2018

water in the subarctic region. Although it is not clear from Fig. 19, the SAT and SST in the subtropical North Pacific around 20ºN are warmer by 2 K in MIROC6 than in MIROC5. Also in the Atlantic, the SAT in the western tropics is warmer in MIROC6. These warmer surface temperatures in MIROC6 indicates a reduction of the cold SAT and SST biases that can be alleviated by an increase in the downward OSR in MIROC6 due to the implementation of a shallow convective parameterization (Fig. 4), and by an increase in eastward transport of the warm pool temperature associated with the stronger STCC in MIROC6 (Fig. 18).

On the other hand, the warm SAT and SST biases in the Southern Ocean and the warm SAT bias in Middle East and the Mediterranean are worse in MIROC6 than in MIROC5. Consequently, the RMS error in SAT is larger in MIROC6 (2.4 K) than in MIROC5 (2.2 K). The former is due essentially to the underestimate of mid-level cloud covers, excess downward OSR, and the resultant underestimate of the sea ice in the Southern Ocean. Such bias commonly occurs in many of climate models and is normally attributed to errors in cloud radiative processes (e.g., Bodas-Salcedo et al., 2012; Williams et al., 2013). In addition, poor representations of mixed layer depths and open ocean deep convections due to the lack of mesoscale processes in the Antarctic Circumpolar Current are causes of the warm bias (Olbers et al., 2004; Downes and Hogg, 2013). The latter warm bias, seen in Middle East around the Mediterranean, can be explained by a tendency to underestimate the cooling effects of aerosol-radiation interactions due to underestimate of dust emissions from the Sahara Desert in MIROC6 (not shown).

3.2 Internal climate variations

3.2.1 Madden-Julian oscillation and East Asian Monsoon

In this section, we will evaluate the reproducibility of internal climate variations in MIROC6 in comparison with MIROC5 and observations, beginning with an examination of the equatorial waves in the atmosphere. Zonal wavenumber–frequency power spectra normalized by background spectra for the symmetric component of OLR are calculated following Wheeler and Kiladis (1999) and are shown in Fig. 20. The daily-mean OLR data derived from the Advanced Very High-Resolution Radiometer (AVHRR) of the National Oceanic and Atmospheric Administration (NOAA) satellites (Liebmann and Smith, 1996; the data are available at https://www.esrl.noaa.gov/psd/data/gridded/data.interp_OLR.html) are used for observational references. The signals corresponding to the Madden-Julian oscillation (MJO), equatorial Kelvin (EK), and Rossby waves (ER) stand out from the background spectra in observations. MIROC5 qualitatively reproduces these spectral maxima qualitatively, while the amplitudes of the MJO and the EK are underestimated. These underestimates are partially mitigated in MIROC6. The power summed over the eastward wavenumber 1–3 and periods of 30–60 days corresponding to the MJO are 20% larger in MIROC6 than in MIROC5. Furthermore, some additional analyses indicate that many aspects of the MJO, including its eastward propagation over the western tropical Pacific, are improved in MIROC6. Those improvements are primarily associated with the implementation of the shallow convective scheme that moistens the lower troposphere. The results of these additional analyses, along with and some sensitivity experiments, are described in a separate paper (Hirota et al., 2018).

Figure 21 shows the June–August (JJA) climatology of precipitation and circulations in the East Asia. As shown in observations (ERA-I; Fig. 21a), the East Asian summer monsoon (EASM) is characterized by the monsoon low over the warmer Eurasian continent and the subtropical high over the colder Pacific Ocean (e.g., Ninomiya and Akiyama, 1992). The southwesterly between these pressure systems transports moist air to the mid-latitudes forming a rainband called *Baiu* in Japanese. The general circulation pattern of the EASM and the rainband are well simulated in both MIROC6 and MIROC5. It should be noted that one of major deficiencies in MIROC5, the underestimate of the precipitation around the Philippines, has been largely alleviated in MIROC6. This improvement is, again, associated with the moistening of the lower troposphere by shallow convective processes. Interannual EASM variabilities are examined using an empirical orthogonal function (EOF) analysis of vorticity at the 850 hPa pressure level over [100°E–150°E, 0°N–60°N] following Kosaka and Nakamura (2010). The regressions of precipitation and 850hPa vorticity with respect to the time series of the first mode (EOF1) are shown in the lower panels of Fig. 21. In observations, precipitation and vorticity anomalies show a tripolar pattern with centers located around the Philippines, Japan, and the Sea of Okhotsk (Hirota and Takahashi, 2012). The anomalies around the Philippines and Japan correspond to the so-called Pacific-Japan pattern (Nitta et al., 1987). In MIROC6, the southwest-northeast orientation of the wave-like anomalies is better simulated in MIROC6 than in MIROC5.

Figure 22 shows the wintertime (December–February) climatology of circulations and the STA in the East Asia. The East Asian winter monsoon (EAWM) is characterized by northwesterly between the Siberian high and the Aleutian low in observations (ERA-I; e.g. Zhang et al., 1997). The monsoon northwesterly advects cold air to East Asia, enhancing the meridional temperature gradients and strengthening the subtropical jet around Japan. The jet's strength influences synoptic wave activities in the storm track. MIROC5 captures the circulation pattern, but significantly underestimates the STA. The STA in MIROC6 is better simulated than in MIROC5, but it is still smaller than in observations. Interannual variability of the EAWM is also better represented in MIROC6 than in MIROC5. The dominant variability of the monsoon northwesterly is extracted as the EOF1 of the meridional wind at the 850 hPa pressure level over the region [30°N–60°N, 120°E–150°E]. In observations, the regressions with respect to the time series of the EOF1 show stronger northwesterly accompanied with suppressed STA, which is consistent with previous studies (Fig. 22d; e.g., Nakamura, 1992). This relationship between the circulations and the STA can be found in MIROC6 but not in MIROC5 (Figs. 22e, f). The explained variance of the EOF1 is 46.0% in observations, 37.1% in MIROC5, and 47.1% in MIROC6, suggesting that the amplitude of this variability in MIROC6 has become closer to observations.

3.2.2 Stratospheric circulations

A few of the major changes in the model setting from MIROC5 to MIROC6 are higher vertical resolution and higher model top altitude in MIROC6, namely, representation of the stratospheric circulations. Here, we examine representation of the Quasi-Biennial Oscillations (QBOs) in MIROC6. Figure 23 shows the time-height cross-sections of the monthly mean, zonal-mean zonal wind over the equator for observations (ERA-I) and MIROC6. In this figure, an obvious QBO with mean period of approximately 22 months can be seen in MIROC6. The mean period is slightly shorter than that of ~28 months in observations, and the simulated QBO period varies slightly from cycle to cycle. The maximum speed of the easterly at the 20 hPa pressure level is approximately -25 m s^{-1} in MIROC6 and that of the westerly is 15 m s^{-1}. On the other hand, the observed maximum wind speeds are -35 m s^{-1} for the easterly and 20 m s^{-1} westerly, respectively. The simulated QBO has somewhat weaker amplitude in MIROC6 than observations, but the same east-west phase asymmetry. The QBO in the MIROC6 shifts upward compared with that in observations, and the simulated amplitude is larger above the 5 hPa pressure level and smaller in the lower stratosphere. The simulated downward propagation of the westerly shear zones of zonal wind ($\partial\bar{u}/\partial z > 0$, where z is the altitude) is faster than the downward propagation of easterly shear zones $(\partial\bar{u}/\partial z) < 0$, which agrees with observations. The QBOs in MIROC6 are qualitatively similar to that represented in the MIROC-ESM, whic is an Earth system model with a similar vertical resolution that participated in the CMIP5 (Watanabe et al., 2011). Note that nothing resembling a realistic QBO was simulated in the previous low-top version MIROC5, which only has a few vertical layers in the stratosphere.

Recently, Yoo and Son (2016) found that the observed MJO amplitude in the boreal winter is stronger than normal during the QBO easterly phase at the 50 hPa pressure level. They also showed that the QBO exerted greater influence on the MJO than did ENSO. Marshall et al. (2016) pointed out the improvement in forecast skill during the easterly phase of the QBO and indicated that the QBO could be a potential source of the MJO predictability. MIROC6 successfully simulates both the MJO and QBO in a way that consistent with observations, as mentioned above, but correlations between the QBO and MJO are not clear. One possible reason is smaller amplitude of the simulated QBO in the lowermost stratosphere. The QBO contribution to tropical temperature variation at the 100 hPa pressure level is ~0.1 K in the MIROC6, which is much smaller than the observed value of ~0.5 K (Randel et al., 2000). The simulated QBO has little effects on static stability and vertical wind shear in the tropical upper troposphere.

MIROC6 can also simulate Sudden Stratospheric Warming (SSW), which is a typical intra-seasonal variability in the mid-latitude stratosphere. Figure 24 shows the standard deviation of monthly and zonal-mean zonal wind in February. Here, a prominent variation is observed over the equatorial stratosphere and the extratropical upper stratosphere. These two maxima, which correspond to QBO and polar vortex variability, respectively, are well captured in MIROC6. Although MIROC6 still has biases for magnitude and structure, no variation with a realistic magnitude appears when the stratosphere is not well resolved (Fig. 24c). The improvement in the simulation of the polar vortex variability is closely related to that of the SSW. As shown in the lower panels of Fig. 24, abrupt and short-lived warming events associated with SSW are detected in MIROC6, which are reproduced comparably to observations in terms of magnitude, but are not detected in MIROC5. This is consistent with previous modeling studies that reported the importance of a well-resolved stratosphere for better simulation of stratospheric variability (e.g., Cagnazzo and Manzini, 2009; Charlton-Perez et al., 2013; Osprey et al., 2013). On the other hand, MIROC6 tends to underestimate the frequency of SSW events in December and January, which is a bias found in common with other high-top climate models (e.g., Inatsu et al., 2007; Charlton-Perez et al., 2013; Osprey et al., 2013). It is conjectured that less frequent stationary wave breaking due to overestimate of climatological wind speeds associated with the polar night jet (Fig. 7e) have the effect to reducing the SSW frequency in December and January.

The inclusion of a well-resolved stratosphere in MIROC6 is also considered to be important for improvement in representation of stratosphere-troposphere coupling. In order to evaluate this, we examine the time-development of the Northern Annular Modes (NAM) associated with strongly weakened polar vortex events in the stratosphere. The NAM indices are defined by the first EOF mode of the zonal-mean year-round daily geopotential height anomalies over the Northern Hemisphere and are computed separately at each pressure level (Baldwin and Thompson, 2009). The height anomalies are first filtered by a 10-day low-pass filter to remove transient eddies. Figure 25 shows the composite of time development of the NAM index for weak polar vortex events. The events are determined by the dates on which the 10 hPa NAM index exceeded -3.0 standard deviations (Baldwin and Dunkerton, 2001). Note that the NAM index is multiplied by the square root of the eigenvalue in each level before the composite, that is, the composite having the geopotential height dimension. The weak polar vortex signal in the stratosphere propagates downward to the surface and persists approximately 60 days in the lower stratosphere and upper troposphere. These observational features are well represented in MIROC6 (Figs. 25ab). Although MIROC5 has also captured downward propagating signals, its magnitude is approximately half in the stratosphere, and its persistency is weak in the lower stratosphere and upper troposphere. Therefore, these results strongly indicate that the inclusion of a well-resolved stratosphere in a model is important for representing not only stratospheric variability, but also stratosphere-troposphere coupling.

3.2.3 El Niño/Southern Oscillation and Indian Ocean Dipole mode

Among the various internal climate variabilities on interannual timescales, ENSO is of great importance because it can influence climate not only in tropics but also mid- and high latitudes of both hemispheres through atmospheric teleconnections associated with wave propagations (e.g., Hoskins and Karoly, 1981; Alexander et al., 2002). Here, we describe representation of ENSO and related teleconnection pattern. Figure 26 shows anomalies of SST, precipitation, the 500 hPa pressure height, and the equatorial ocean temperature regressed onto the NINO3 index which is defined as the area average of the SST in [5°S–5°N, 150°W–90°W]. ProjD and ERA-I in 1980–2009 are used as observations. Although the maximum of the SST anomalies in the tropical Pacific is shifted more westward than in observations, the ENSO-related SST anomalies simulated in both of MIROC6 and MIROC5 are globally consistent with observations (Figs. 26a-c). Simulated positive precipitation anomalies in MIROC6 still overextend to the western Pacific (Figs. 26d-f). Meanwhile, dry anomalies over the maritime continent, the eastern equatorial Indian Ocean, and South Pacific Convergence Zone (SPCZ) are better simulated in MIROC6 than in MIROC5. ENSO teleconnection patterns in Z500 (Figs. 26g-i) are also realistically simulated as seen in, for example, the Pacific-North American pattern (Wallace and Gutzler, 1981). Equatorial subsurface ocean temperature anomalies in MIROC6 are more confined within the thermocline than in MIROC5 (Figs. 26j-l), and the signals in MIROC6 are closer to observations. However, the existence depths of the subsurface signals are larger in MIROC6 than in observations. This is due to the difference in the climatological structure of the equatorial thermocline, which is attributed to the overestimate of the trade winds over the equatorial Pacific, as mentioned in Section 3.1.2.

As well as ENSO, the Indian Ocean Dipole (IOD) mode is recognized as a prominent interannual variability (Saji et al., 1999; Webster et al., 1999). Figure 27 shows anomalies of SST, 10 m wind, and precipitation regressed onto the autumn (September–November) dipole mode index (DMI) which is defined as the zonal difference of the anomalous SST averaged over [10°S–10°N, 50°E–70°E] and that averaged in [10°S–10°N, 90°E–110°E]. ProjD and ERA-I in 1980–2009 are used as observations. The observed positive IOD phase is characterized by a basin-wide zonal mode with positive (negative) SST anomalies in the western (eastern) Indian Ocean, and precipitation is increased (decreased) over the positive (negative) SST anomalies (Figs. 27ad). The dipole SST pattern is better simulated in MIROC6 than in MIROC5 where the eastern SST anomalies are located more southward than in observations (Figs. 27a-c). Correspondingly, a meridional dipole pattern in the precipitation of MIROC5 is alleviated, and MIROC6 shows a zonal dipole precipitation pattern, as in observations (Figs. 27d-f). Seasonal IOD phase locking to boreal autumn, which is assessed based on RMS amplitude of the DMI, is also better simulated in MIROC6 than in MIROC5 (not shown). Seasonal shoaling of the eastern equatorial thermocline in the Indian Ocean is realistically simulated in MIROC6 during boreal summer to autumn. The shallower thermocline leads the stronger thermocline feedback which is evaluated based on the SST anomalies regressed onto the 20°C isotherm depth anomalies averaged over the eastern part of the IOD region. As displayed in the top of the upper panels of Fig. 27, the thermocline feedback in MIROC6 is comparable to observations. This larger thermocline feedback in MIROC6 possibly leads to the above-mentioned improvements in the IOD pattern. Note that the simulated surface wind anomalies are more realistic in MIROC6 than in MIROC5, although the magnitude of SST anomalies is overestimated in MIROC6. The overestimate of the SST anomalies may have arisen from an excessive response of the equatorial and coastal Ekman up- and down-welling to the wind changes, which are favorable in coarse-resolution ocean models.

3.2.4 Decadal-scale variations in the Pacific and Atlantic Oceans

On longer-than-interannual timescales, the PDO (Mantua et al., 1997) or the Inderdecadal Pacific Oscillations (IPO; Power et al., 1999) is known to be a dominant climate mode that is detected in the SST and the SLP over the North Pacific. To examine simulated PDO patterns, monthly SST and wintertime (December–February) SLP anomalies are regressed onto the PDO index defined as the 1st EOF mode of the North Pacific SST to the north of 20°N and are shown in Fig. 28. In order to detect the decadal-scale variation, the COBE-SST2/SLP2 data (Hirahara et al., 2014) from 1900 to 2013 are used as observations. Negative SST anomalies in the western and central North Pacific and positive SST anomalies in the eastern North Pacific are found in observations. These signals are also represented in both of MIROC6 and MIROC5. The regression of SLP anomalies corresponding to the deepening of the Aleutian low are well simulated in the models over the subarctic North Pacific, and it can be seen that the amplitudes of the SLP anomalies are larger and better represented in MIROC6 than in MIROC5. In the tropical Pacific, positive SST anomalies, which are among the more important driving processes of the PDO (e.g. Alexander et al., 2002), are seen in both the models and the observations. In MIROC5, the 5-yr running means of the wintertime (November–March) North Pacific Index (NPI), defined as the SLP averaged over [30°N–65°N, 160°E–140°W], are excessively less sensitive to the NINO3 index (correlation coefficient r = -0.37) than to the NINO4 index (r = -0.64). Note that the NINO4 index is defined as the area average of the SST in [5°S–5°N, 160°E–150°W]. The distorted response of the extratropical atmosphere to the tropical SST variations works to unsuitably modify the extratropical ocean and plays a major role in limiting the decadal predictability of the PDO index in MIROC5 (Mochizuki et al., 2014). In contrast, those in MIROC6 are well correlated with the NINO3 index (r = -0.61) in addition to the NINO4 index (r = -0.62). Overestimate of the tropical signals of MIROC5 in the western tropical Pacific are also alleviated in MIROC6. The above-mentioned PDO improvement and the linkage between the tropics and the mid-latitude North Pacific imply a potential for improved skills in initialized decadal climate predictions.

In the Atlantic Ocean, there is another decadal-scale variability, which is called the AMO (Schlesinger and Ramankutty, 2004). Figure 29 shows anomalies of SST and SLP regressed onto the AMO index, which is defined as the area average of the SST anomalies in the North Atlantic [0°–60°N, 0°–80°W] with the global-mean SST anomalies subtracted (Trenberth and Shea, 2006). As in the PDO, the centennial-long data of the COBE-SST2/SLP2 data in 1900–2013 are used as observations. The observed AMO spatial pattern in its positive phase is characterized by positive SST anomalies in the off-equator and the subarctic North Atlantic, and by negative or weakly-positive SST anomalies in the western subtropical North Atlantic (Fig. 29a). Corresponding to negative (positive) SLP anomalies over the subtropical (subarctic) North Atlantic, the mid-latitude westerly jet is weaker in a positive AMO phase than in normal years. These spatial patterns in the SST and SLP are simulated in both of MIROC6 and MIROC5. It is especially noteworthy that the positive SST anomalies in low latitudes have larger amplitudes in MIROC6 than in MIROC5, and they extend to the South Atlantic as in observations (Figs. 29bc). On the other hand, the positive SST anomalies in the subarctic region are underestimated in MIROC6, which may be due to the smaller RMS amplitudes of NADW transport in MIROC6 (see Section 3.1).

3.3 Climate sensitivity

Following the regression method by Gregory et al. (2004) and Gregory and Webb (2008), we conducted abrupt CO_2 quadrupling experiments with MIROC6 and MIROC5 in order to evaluate effective climate sensitivity (ECS), radiative forcing, and climate feedback. The CO_2 quadrupling experiments were initiated from the pre-industrial control runs. Data from the first 20 years after the CO_2 increase were used for the analysis.

ECS, $2 \times CO_2$ radiative forcing, and climate feedback for MIROC6 are estimated to be 2.5 K, 3.8 Wm^{-2}, and -1.5 Wm^{-2}, respectively (Fig. 30a and Table 2). The ECS, radiative forcing, and climate feedback in MIROC6 are lower, higher, and negatively larger than those of the CMIP5 multi-model ensemble means, although these estimates for MIROC6 are within the ensemble spreads of the multi-models (Andrews et al., 2012). The ECS of MIROC6 is almost the same as MIROC5 because the decrease in radiative forcing is counterbalanced by the positive increase in climate feedback, although the change in climate feedback is small and not statistically significant. The decrease in

Geosci. Model Dev. Discuss., https://doi.org/10.5194/gmd-2018-155
Manuscript under review for journal Geosci. Model Dev.
Discussion started: 16 July 2018

radiative forcing of MIROC6 relative to MIROC5 is evident in the longwave and shortwave cloud components (LCRE and SCRE in Fig. 30b and Table 3). On the other hand, the clear-sky shortwave component (SWclr) increases in MIROC6 relative to MIROC5, which partially cancels the differences between the two models. The positive increase in climate feedback is pronounced in the SCRE, which is partially offset by the decrease in the clear sky longwave (LWclr) and SWclr (Fig. 30c and Table 3).

We now focus on the SCRE of the radiative forcing and climate feedback, which show the largest differences between the two models, and compare the geographical distribution (Fig. 31). The distribution is calculated by regressing the changes in SCRE caused by the CO_2 increase at each latitude-longitude grid box against the change in the global-mean SAT. There is a large difference in the geographical distribution between MIROC6 and MIROC5, with the former showing more pronounced zonal contrast in the tropical Pacific than the latter. The changes in the global mean from MIROC5 to MIROC6 (Figs. 30bc) are consistent with the changes in the western tropical Pacific, showing more negative radiative forcing and more positive climate feedback, which are partially offset by the changes in the central tropical Pacific with opposite signs. Interestingly, the radiative forcing and climate feedback tend to show similar geographical patterns with opposite signs in each model.

4. Summary and discussions

The sixth version of a climate model, MIROC6, was developed by a Japanese climate modeling community, aiming at contributing to the CMIP6 through deeper understanding of a wide range of climate science issues and seasonal-to-decadal climate predictions and future climate projections. The model configurations and basic performances in the pre-industrial control simulation have been described and evaluated in the present manuscript. Major changes from MIROC5, which was our official model for the CMIP5, to MIROC6 are mainly done in the atmospheric component. These include implementation of a parameterization of shallow convective processes, the higher model

TOA, vertical resolution in the stratosphere. The ocean and land-surface components have been also updated in terms of the horizontal grid coordinate system and higher vertical resolution in the former, and parameterizations for sub-grid scale snow distribution and wet lands due to snow-melting water in the latter. Overall, the model climatology and internal climate variability of MIROC6, which are assessed in comparison with observations, are better simulated than in MIROC5.

Overestimate of low-level cloud amounts in low latitudes, which can be partly attributed to insufficient representation of shallow convective processes, are significantly alleviated in MIROC6. The free atmosphere becomes wetter and the precipitation over the western tropical Pacific becomes larger in MIROC6 than in MIROC5, primarily due to vertical mixing of the humid air in the planetary boundary layer with the dry air in the free troposphere. Shallow convections also contribute to better propagation characteristics of intra-seasonal variability associated with MJO in MIROC6, as well as East Asian summer monsoon variability on interannual timescales. In addition, QBO, which is absent in MIROC5, appears in MIROC6 because of its better stratospheric resolution and non-orographic gravity wave drag parameterization.

Climatic mean and internal climate variability in the mid-latitudes are also remarkably improved in MIROC6. Together with enhanced activity of sub-weekly disturbances, the tropospheric westerly jets in MIROC6 are shifted more poleward and are stronger than in MIROC5, especially in the Northern Hemisphere. Overestimates in zonal wind speed of the polar night jet are reduced in MIROC6. These advanced representations lead to tighter interactions between the troposphere and the stratosphere in MIROC6. SSW events in the form of polar vortex destructions induced by upward momentum transfer from the troposphere to the stratosphere (e.g., Matsuno, 1971), are well captured in MIROC6. On interannual timescales, the improvement of the westerly jet results in better representations of the spatial wind pattern of the wintertime East Asian monsoon. Associated with changes in the large-scale atmospheric circulations, the western boundary currents in the oceans, the

Geosci. Model Dev. Discuss., https://doi.org/10.5194/gmd-2018-155
Manuscript under review for journal Geosci. Model Dev.
Discussion started: 16 July 2018

Geoscientific Model Development Discussions
Open Access

Kuroshio-Oyashio current system, the Gulf Stream, and their extensions are better simulated in MIROC6. The increase in warm water transport from the subtropical North Atlantic to the Barents Sea seems to melt the sea ice in the Barents Sea, and to alleviate the overestimate of the wintertime sea-ice area that is seen in that region in MIROC5. Another remarkable improvement in MIROC6 is found in the climatological snow cover fractions in the early winter over the Northern Hemisphere continents. In the Southern Hemisphere, however, the underestimate of mid-level clouds and the corresponding warm SAT bias, the underestimate of sea-ice area, and the overestimate of incoming shortwave radiation in the Southern Ocean, all of which are attributed to errors in cloud radiative and planetary boundary layer processes (e.g., Bodas-Salcedo et al., 2012; Williams et al., 2013), remains the same as in MIROC5.

Qualitatively, the linkage representations between the tropics and the mid-latitudes associated with ENSO in MIROC6 are mostly the same as in MIROC5, qualitatively. Meanwhile, oceanic subsurface signals, which partly control ENSO characteristics, are more confined along the equatorial thermocline in MIROC6, which is consistent with observations. Regarding the PDO, tropical influence on the mid-latitudes is more dominant in MIROC6 than in MIROC5, suggesting improvements in decadal-scale atmospheric teleconnections in MIROC6.

The above descriptions are mainly on the Pacific internal climate variabilities. Regarding the Indian Ocean, the zonal dipole structures in the SST and precipitation associated with the interannual variability, known as the IOD, are better simulated in MIROC6 than in MIROC5, which has a bias of a false meridional precipitation pattern. In the Atlantic, the multi-decadal variability, known as the AMO, is represented in both of the models roughly consistent with observations, but their reproducibility shows both drawbacks and advantage. Signals associated with AMO in the subarctic (tropical) region are underestimated (overestimated) in MIROC6 (MIROC5).

As one of important metrics for quantifying uncertainty in future climate projections, ECS

Geosci. Model Dev. Discuss., https://doi.org/10.5194/gmd-2018-155
Manuscript under review for journal Geosci. Model Dev.
Discussion started: 16 July 2018

Geoscientific Model Development Discussions
Open Access

is also estimated. Although the model configurations and performances are different between the models, the ECS is almost the same (2.5 K). However, looking at geographical distributions of radiative forcing and climate feedback, the amplitudes of shortwave cloud components are much larger in MIROC6 than in MIROC5. Since the larger negative (positive) radiative forcing and positive (negative) climate feedback in the western (central) tropical Pacific cancel each other, global-mean quantities in MIROC6 almost remain the same as in MIROC5. As a topic of future study, estimating radiative forcing and climate feedback with Atmospheric Model Intercomparison Project-type experiments in order to check robustness of the present study would be desirable. Elucidating the impact of different geographical patterns of radiative forcing and climate feedback on the projected future climates would also be useful.

After conducting the pre-industrial control simulation and evaluating the model reproducibility of the mean climate and the internal climate variability, ensemble historical simulations that were initiated from the pre-industrial simulations were executed using the historical forcing data recommended by the CMIP6 protocol. Figure 32 shows a time series of the global-mean SAT anomalies with respect to the 1961–1990 mean. There are 10 (5) ensemble members in the MIROC6 (MIROC5) historical simulations. Note that the MIROC5 historical simulations are executed using the forcing datasets of the CMIP5 protocol. As shown in Fig. 32, the simulated SAT variations in both of MIROC6 and MIROC5 follow observations (HadCRUTv4.4.0; Morice et al., 2012; the data are available at https://crudata.uea.ac.uk/cru/data/temperature/) on a centennial timescale. The temperature rises from the nineteenth century to the early twenty-first century are about 0.72 K in MIROC6, 0.85 K in MIROC5, and 0.82 K in observations, respectively. Focusing on the period from the 1940s to the 1960s, the SAT variations seem to be better simulated in MIROC6 than in MIROC5, which can be due to both of an update of the forcing datasets and the larger ensemble number in MIROC6. On the other hand, the warming trend during the first half of the twentieth century in the

Geosci. Model Dev. Discuss., https://doi.org/10.5194/gmd-2018-155
Manuscript under review for journal Geosci. Model Dev.
Discussion started: 16 July 2018

Geoscientific Model Development Discussions Open Access

models is about half as large as in observations. Whether it can be attributed to internal climate variability (e.g., Thompson et al., 2014; Kosaka and Xie, 2016) or to an externally forced mode (e.g., Meehl et al., 2003; Nozawa et al., 2005) is still being debated. Interestingly, the so-called recent hiatus of the global warming (Easterling and Wehner, 2009) in the first decade of the twenty-first century is reasonably captured in MIROC6. The observed hiatus is considered to occur in association with a negative IPO phase (e.g., Meehl et al., 2011; Watanabe et al., 2014), while the simulated spatial pattern of the SAT trends in the first decade of the twenty-first century does not have a negative IPO pattern (not shown). Considering that the ensemble mean of the individual simulations reflects only externally-forced variations and that signals of internal climate variations have been roughly removed, the simulated hiatus in MIROC6 could be spurious and the SAT trend difference between MIROC6 and MIROC5 could be attributed to the difference in the forcing datasets.

As summarized above, the overall reproducibility of the mean climate and the internal variability in the latest version of our climate model, MIROC6, has progressed, as well as the historical warming trend of the climate system. During the first trial of the preindustrial simulation conducted just after the model configuration was frozen, however, the model reproducibility was not as good as seen in MIROC5. As described in Section 2.5, we intensively tuned the model by perturbing parameters associated with, especially, cumulus and shallow convections, and planetary boundary processes. In addition, before starting the historical simulations, we estimated and tuned the cooling effects due to aerosol-radiation and aerosol-cloud interactions by changing the parameters of cloud microphysics in order to ensure that the estimated cooling would be closer to the best-estimate of the IPCC-AR5 (IPCC, 2013). Without this parameter tuning, the simulated warming trend after the 1960s was 70% as large as seen in observations. This dependence of radiative forcing and reproducibility of the warming trend on cloud microphysics has also been reported in other climate models (Golaz et al., 2013). A recent comparison of cloud mircophysical statistics between climate models and satellite-

Geosci. Model Dev. Discuss., https://doi.org/10.5194/gmd-2018-155
Manuscript under review for journal Geosci. Model Dev.
Discussion started: 16 July 2018

Geoscientific Model Development Discussions
Open Access

based observations has pointed out that "tuned" model parameters that were adjusted for adequate radiative cooling and realistic SAT changes do not necessarily ensure cloud properties and rain/snow formations will be consistent with observations and implies the presence of error compensations in climate models (e.g., Suzuki et al., 2013; Michibata et al., 2016). Error compensations are found also in both of global and regional aspects. As described in Section 3.1, the global TOA radiation imbalance in MIROC6 is about -1.1 Wm^{-2}, which is consistent with -0.8 Wm^{-2} in observations. However, when the TOA imbalance is examined in parts, cloud radiative components in the model contain non-negligible biases with respect to satellite-based observations. Regarding the Pacific Ocean, the northward transport of CDW is about 8.6 Sv and is within the uncertainty range of observations. Although this transport is realistic, it is maintained by open ocean convections in the Southern Ocean, which occur apart from the coastal region of Antarctica and reach the sea floor, that are artifacts in coarse-resolution ocean models where oceanic mesoscale eddies and coastal bottom water formation cannot be represented (e.g., Olbers et al., 2004; Downes and Hogg, 2013).

There remain several key foci of ongoing model development efforts. These include process-oriented refinements of cloud microphysics and convective systems based on constraints from satellite data and feedbacks from cloud-resolving atmospheric models (e.g., Satoh et al., 2014), higher resolutions for representations of regional extremes, oceanic eddies and river floods, and parameterization of tide-induced micro-scale mixing of sea water. Improvement of computational efficiency, especially on massive parallel computing systems, is among the urgent issues for long-term and large ensemble simulations. In terms of model architecture, giving each sub-module in a climate model greater independence for effective model development may be required. These improvements can contribute to deeper understanding of the Earth's climate, reducing uncertainties in climate projections and predictions, and more precise evaluations of human influences on carbon-nitrogen cycles when applied to Earth system models.

Geosci. Model Dev. Discuss., https://doi.org/10.5194/gmd-2018-155
Manuscript under review for journal Geosci. Model Dev.
Discussion started: 16 July 2018

Code and data availability. Source code of MIROC6 and MIROC5 associated with this study is available to those who conduct collaborative research with the model users under license from copyright holders. For further information on how to obtain the code, please contact the corresponding author. The data from the model simulations and observations used in the analyses are available from the corresponding author upon request.

Competing interests. The authors declare that they have no conflict of interest.

Acknowledgements

This research is supported by the "Integrated Research Program for Advancing Climate Models (TOUGOU Program)" from the Ministry of Education, Culture, Sports, Science, and Technology (MEXT), Japan. Model simulations were performed on the Earth Simulator at JAMSTEC and NEC SX-ACE at NIES. The authors are much indebted to Dr. Teruyuki Nishimura and Mr. Hiroaki Kanai for their long-term support in areas related to model developments and server administration. The authors also wish to express thanks to our anonymous reviewers for their suggestions and careful reading of the manuscript.

References

Adcroft, A., Hill, C., and Marshall, J.: Representation of topography by shaved cells in a height coordinate ocean model, Mon. Wea. Rev., 125, 2293–2315, 1997.

Adler, R. F., Huffman, G. J., Chang, A., Ferraro, R., Xie, P., Janowiak, J., Rudolf, B., Schneider, U., Curtis, S., Bolvin, D., Gruber, A., Susskind, J., and Arkin, P.: The Version 2 Global Precipitation Climatology Project (GPCP) Monthly Precipitation Analysis (1979–Present), J. Hydrometeor., 4,

Geosci. Model Dev. Discuss., https://doi.org/10.5194/gmd-2018-155
Manuscript under review for journal Geosci. Model Dev.
Discussion started: 16 July 2018

Geoscientific Model Development Discussions
Open Access
EGU

1147–1167, 2003.

Alexander, M. A., Bladé, I., Newman, M., Lanzante, J. R., Lau, N.-C., and Scott, J. D.: The atmospheric bridge: The influence of ENSO teleconnections on air–sea interaction over the global oceans, J. Clim., 15, 2205–2231, 2002.

Andrews, T., Foster, P., Boucher, O., Bellouin, N., and Jones, A.: Precipitation, radiative forcing and global temperature change. Geophys. Res. Lett., 37, doi:10.1029/2010GL043991, 2010.

Andrews, T., Gregory, J. M., Webb, M. J., and Taylor, K. E.: Forcing, feedbacks and climate sensitivity in CMIP5 coupled atmosphere-ocean climate models, Geophys. Res. Lett., 39, L09712, doi:10.1029/2012GL051607, 2012.

Arakawa, A. and Konor, C. S.: Vertical differencing of the primitive equations based on the Charney-Phillips grid in hybrid σ-p vertical coordinates, Mon. Wea. Rev., 124, 511-528, 1996.

Baldwin, M. P. and Dunkerton, T. J.: Stratospheric harbingers of anomalous weather regimes, Science, 294, 581-584, 2001.

Baldwin, M. P. and Thompson, D. W. J.: A critical comparison of stratosphere-troposphere coupling indices, Quart. J. Roy. Meteorol. Soc., 135, 1661–1672, 2009.

Bamber, J. L. and Aspinall, W. P.: An expert judgement assessment of future sea level rise from the ice sheets, Nature Clim. Change, 3, 424–427, 2013.

Baran, A. J.: From the single-scattering properties of ice crystals to climate prediction: A way forward, Atmospheric Res., 112, 45-69, 2012.

Bengtsson, L., Hodges, K. I., and Keenlyside, N.: Will extratropical storms intensify in a warmer climate? J. Clim., 22, 2276-2301, 2009.

Bitz, C., Holland, M., Weaver, A., and Eby, M.: Simulating the ice-thickness distribution in a coupled climate model, J. Geophys. Res., 106, 2441–2463, 2001.

Bryan, K.: Accelarating the convergence to equilibrium of ocean-climate models, J. Phys. Oceanogr.,

Geosci. Model Dev. Discuss., https://doi.org/10.5194/gmd-2018-155
Manuscript under review for journal Geosci. Model Dev.
Discussion started: 16 July 2018

14, 666-673.

Brodzik, M. and Armstrong, R.: Northern Hemisphere EASE-Grid 2.0 Weekly Snow Cover and Sea Ice Extent. Version 4, Boulder, Colorado USA: NASA DAAC at the National Snow and Ice Data Center, 2013.

Cagnazzo, C. and Manzini, E.: Impact of the stratosphere on the winter tropospheric teleconnections between ENSO and the North Atlantic and European region, J. Clim., 22, 1223-1238, 2009.

Carton, J. A. and Giese, B. S.: A reanalysis of ocean climate using simple ocean data assimilation, Mon. Wea. Rev., 136, 2999–3017, 2008.

Cavarieli, D. J., Corawford, J. P., Drinkwater M. R., Eppler, D. T., Farmer, L. D., Jentz, R. R., and Wackerman, C. C.: Aircraft active and passive microwave validation of sea ice concentrations from the DMSP SSM/I, J. Geophy. Res., 96, 21989-22088, 1991.

Charlton-Perez, A. J., and co-authors: On the lack of stratospheric dynamical variability in low-top versions of the CMIP5 models, J. Geophys. Res., 118, 2494-2505, 2013.

Chikamoto, Y., Timmermann, A., Luo, J.-J., Mochizuki, T., Kimoto, M., Watanabe, M., Ishii, M., Xie, S.-P., and Jin, F.-F.: Skillful multi-year predictions of tropical trans-basin climate variability, Nature. commun., 6, doi:10.1038/ncomms7869, 2015.

Chikira, M. and Sugiyama, M.: A cumulus parameterization with state-dependent entrainment rate. Part I: Description and sensitivity to temperature and humidity profiles, J. Atmos. Sci., 67, 2171-2193, 2010.

Church, J. A. and White, N. J.: Sea-level rise from the late 19th to the early 21st century, Surv. Geophys., 32, 585–602, 2011.

Comiso, J. C., Parkinson, C. L., Gersten, R., and Stock, L.: Accelerated decline in the Arctic sea ice cover, Geophys. Res. Lett., 35, doi:10.1029/2007GL031972, 2008.

Dee, D.. and co-authors: The ERA-Interim reanalysis: configuration and performance of the data

Geosci. Model Dev. Discuss., https://doi.org/10.5194/gmd-2018-155
Manuscript under review for journal Geosci. Model Dev.
Discussion started: 16 July 2018

assimilation system. Quart J Roy Met. Soc., 137, 535–597, 2011.

Downes, S. M. and Hogg, A. M.: Southern Ocean circulation and eddy compensation in CMIP5 models, J. Clim., 26, 7198-7220, 2013.

Easterling, D. R. and Wehner, M. F.: Is the climate warming or cooling? Geophys. Res. Lett., 36, doi:10.1029/2009GL037810, 2009.

Eyring, V., Bony, S., Meehl, G. A., Senior, C. A., Stevens, B., Stouffer, R. J., and Taylor, K. E.: Overview of the Coupled Model Intercomparison Project Phase 6 (CMIP6) experimental design and organization, Geosci. Model. Dev., 9, 1937-1958, 2016.

Gantt, B., Meskhidze, N., and Kamykowski, D.: A new physically-based quantification of marine isoprene and primary organic aerosol emissions, Atmos. Chem. Phys., 9, 4915-4927, doi:10.5194/acp-9-4915-2009, 2009.

Gantt, B., Meskhidze, N., Facchini, M. C., Rinaldi, M., Ceburnis, D., and O'Dowd, C. D.: Wind speed dependent size-resolved parameterization for the organic mass fraction of sea spray aerosol, Atmos. Chem. Phys., 11, 8777-8790, doi:10.5194/acp-11-8777-2011, 2011.

Gent, P.R., Willebrand, J., McDougall, T.J., and McWilliams, J.C: Parameterizing eddy-induced tracer transports in ocean circulation models, J. Phys. Oceanogr., 25, 463-474, 1995.

Golaz, J. C., Horowitz, L. W., and Levy II, H.: Cloud tuning in a coupled climate model: Impact on 20th century warming, Geophys. Res. Lett., 40, 2246-2251, 2013.

Gregory, D.: Estimation of entrainment rate in simple models of convective clouds, Quart. J. Roy. Meteor. Soc., 127, 53–72, 2001.

Gregory, J. M., Ingram, W. J., Palmer, M. A., Jones, G. S., Stott, P. A., Thorpe, R. B., Lowe, J. A., Johns, T. C., and Williams, K. D.: A new method for diagnosing radiative forcing and climate sensitivity, Geophys. Res. Lett., 31, L03205, doi:10.1029/2003GL018747, 2004.

Gregory, J. and Webb, M.: Tropospheric adjustment induces a cloud component in CO2 forcing, J.

Geosci. Model Dev. Discuss., https://doi.org/10.5194/gmd-2018-155
Manuscript under review for journal Geosci. Model Dev.
Discussion started: 16 July 2018

Geoscientific Model Development Discussions
Open Access

Clim., 21, 58-71, 2008.

Griffies, S. M., Gnanadesikan, A., Dixon, K. W., Dunne, J. P., Gerdes, R., Harrison, M. J., Rosati, A., Russell, J. L., Samuels, B. L., Spelman, M. J., Winton, M., and Zhang, R.: Formulation of an ocean model for global climate simulations, Ocean Sci., 1, 45-79, 2005.

Guenther, A., Hewitt, N., Erickson, D., Fall, R., Geron, C., Graedel, T., Harley, P., Klinger, L., Lerdau, M., McKay, W., Pierce, T., Scholes, B., Steinbrecher, R., Tallamraju, R., Taylor, J., and Zim-merman, P.: A global model of natural volatile organic compound emissions, J. Geophys. Res., 100, 8873–8892, 1995.

Hasumi, H.: CCSR Ocean Component Model (COCO) version 4.0, Center for Climate System Research Rep., 25, 103 pp., 2006. [Available online at http://www.ccsr.u-tokyo.ac.jp/hasumi/COCO/coco4.pdf.]

Hegglin, M. I., and co-authors: Historical and future ozone database (1850-2100) in support of CMIP6, in prep.

Hines, C. O.: Doppler-spread parameterization of gravity wave momentum deposition in the middle atmosphere, Part 2: Broad and quasi monochromatic spectra, and implementation, J. Atmos. Solar Terr. Phys., 59, 387–400, 1997.

Hirahara, S., Ishii, M., and Fukuda, Y.: Centennial-scale sea surface temperature analysis and its uncertainty, J. Clim., 27, 57-75, 2014.

Hirota, N., Ogura, T., Tatebe, H., Shiogama, H., Kimoto, M., and Watanabe, M.: Roles of shallow convective moistening in the eastward propagation of the MJO in MIROC6, J. Clim., 31, 3033-3034, 2018.

Hirota, N. and Takahashi, M.: A tripolar pattern as an internal mode of the East Asian summer monsoon, Clim. Dyn., 39, 2219–2238, doi:10.1007/s00382-012-1416-y, 2012.

Hoesly, R.M., and co-authors: Historical (1750-2014) anthropogenic emissions of reactive gases and

Geosci. Model Dev. Discuss., https://doi.org/10.5194/gmd-2018-155
Manuscript under review for journal Geosci. Model Dev.
Discussion started: 16 July 2018

Geoscientific Model Development Discussions
Open Access

aerosols from the Community Emission Data System (CEDS), Geosci. Model Dev., 11, 369-408, doi:10.5194/gmd-11-369-2018, 2018.

Hourdin, F., Maurisen, T., Getteleman, A., Golaz, J.-C., Balaji, V., Duan, Q., Folini, D., Klocke, D., Qian, Y., Rauser, F., Rio, C., Tomassini, L., Watanabe, M., and Williamson, D.: The art and science of climate model tuning, Bull. Amet. Meteor. Soc., 98, 589-602, 2017.

Hoskins, B. J. and Karoly, D. J.: The steady linear response of a spherical atmosphere to thermal and orographic forcing, J. Atmos. Sci., 38, 1179-1196, 1981.

Hunke, E. and Dukowicz, J.: An elastic–viscous–plastic model for sea ice dynamics, J. Phys. Oceanogr., 27, 1849–1867, 1997.

Hurtt, G., and co-authors: Harmonization of global land-use change and management for the period 850-2100, Geosci. Model Dev., in preparation.

Inatsu, M., Kimoto, M. and Sumi, A.: Stratospheric sudden warming with projected global warming and related tropospheric wave activity, SOLA, 3, 105-108, 2007.

Ineson, S. and Scaife, A. A.: The role of the stratosphere in the European climate response to El Niño, Nature Geosci., 2, 32-36, 2009.

IPCC: Climate Change 2007: The Physical Science Basis. Contribution of Working Group I to the Fourth Assessment Report of the Intergovernmental Panel on Climate Change, edited by Solomon, S., Qin, D., Manning, M., Chen, Z., Marquis, M., Averyt, K. B., Tignor, M. and Miller, H. L., Cambridge University Press, Cambridge, United Kingdom and New York, NY, USA, 996 pp.

IPCC: Climate Change 2013: The Physical Science Basis. Contribution of Working Group I to the Fifth Assessment Report of the Intergovernmental Panel on Climate Change, edited by Stocker, T.F. et al., Cambridge University Press, Cambridge, United Kingdom and New York, NY, USA, 1535 pp, 2013.

Ishii, M., Kimoto, M., and Kachi, M.: Historical ocean subsurface temperature analysis with error

Geosci. Model Dev. Discuss., https://doi.org/10.5194/gmd-2018-155
Manuscript under review for journal Geosci. Model Dev.
Discussion started: 16 July 2018

Geoscientific Model Development Discussions
Open Access

estimate, Mon. Wea. Rev., 131, 51-73, 2003.

Imada, Y., Watanabe, M., Mori, M., Kimoto, M., Shiogama, H., and Ishii, M.: Contribution of atmospheric circulation change to the 2012 heavy rainfall in southwestern Japan, Bull. Amer. Meteor. Soc., 95, S52-S54, 2013.

Imada, Y., Tatebe, H., Ishii, M., Chikamoto, Y., Mori, M., Arai, M., Watanabe, M., and Kimoto, M.: Predictability of two types of El-Niño assessed using an extended seasonal prediction system by MIROC, Mon. Wea. Rev., 143, 4597-4617, 2015.

Ito, A. and Inatomi, M.: Use of a process-based model for assessing the methane budgets of global terrestrial ecosystems and evaluation of uncertainty, Biogeosciences, 9, 759-773, 2012.

K-1 model developers: K-1 coupled GCM (MIROC) description, K-1 Tech. Rep., 1, edited by H. Hasumi, H., and Emori, S., 34 pp., Center for Climate System Research, the Univ. of Tokyo, Tokyo, 2004.

Kamae, Y., Shiogama, H., Watanabe, M., Ogura, T., Yokohata, T., and Kimoto, M.: Lower tropospheric mixing as a constraint on cloud feedback in a multiparameter multiphysics ensemble, J. Clim., 29, 6259-6275, 2016.

Katsumate, K., Ohshima, K. I., Kono, T., Itoh, M., Yasuda, I., Volkov, Y., and Wakatsuchi, M.: Water exchange and tidal current through the Bussol's Strait revealed by direct current measurements, J. Geophys. Res., 109, doi:10.1019/2003JC001864, 2004.

Kawabe, M. and Fujio, S.: Pacific Ocean circulation based on observation, J. Oceanogr., 66, 389-403, doi:10.1007/s10872-010-0034-8, 2010.

Krinner, G., Viovy, N., de Noblet-Ducoudre, N., Ogee, J., Polcher, J., Friedlingstein, P., Ciais, P., Sitch, S., and Prentice, I. C.: A dynamic global vegetation model for studies of the coupled atmosphere-biosphere system, Global Biogeochem. Cycles, 19, GB1015, doi:10.1029/2003GB002199, 2005.

Komuro, Y., Suzuki, T., Sakamoto, T. T., Hasumi, H., Ishii, M., Watanabe, M., Nozawa, T., Yokohata,

Geosci. Model Dev. Discuss., https://doi.org/10.5194/gmd-2018-155
Manuscript under review for journal Geosci. Model Dev.
Discussion started: 16 July 2018

T., Nishimura, T., Ogochi, K., Emori, S., and Kimoto, M.: Sea-ice in twentieth-century simulations by new MIROC coupled models: a comparison between models with high resolution and with ice thickness distribution, J. Meteor. Soc. Japan, 90A, 213–232, 2012.

Komuro, Y. and Suzuki, T.: Impact of subgrid-scale ice thickness distribution on heat flux on and through sea ice, Ocean Modell., 71, 13–25, 2013.

Komuro, Y.: The Impact of Surface Mixing on the Arctic River Water Distribution and Stratification in a Global Ice–Ocean Model, J. Clim., 27, 4359-4370, 2014.

Kosaka, Y. and Nakamura, H.: Mechanisms of meridional teleconnection observed between a summer monsoon system and a subtropical anticyclone. Part I: The Pacific-Japan pattern, J. Clim., 23, 5085–5108, 2010.

Kosaka, Y, and Xie, S.-P.: The tropical Pacific as a key pacemaker of the variable rates of global warming, Nature Geosci., 9, 669-673, 2016.

Kubokawa, A., and Inui, T.: Subtropical Countercurrent in an idealized Ocean OGCM, J. Phys. Oceanogr., 29, 1303-1313, 1999.

Liebmann, B.: Description of a complete (interpolated) outgoing longwave radiation dataset, Bull. Amer. Meteor. Soc., 77, 1275–1277, 1996.

Liston, G.E.: Representing subgrid snow cover heterogeneities in regional and global models, J. Clim., 17, 1381-1397, 2014.

Loeb, N. G., Wielicki, B. A., Doelling, D. R., Smith, G.L., Keyes, D.F., Kato, S., Manalo-Smith, N., and Wong, T.: Toward optimal closure of the earth's top-of-atmosphere radiation budget, J. Clim., 22, 748–766, 2009.

Mantua, N. J., Hare, S. R., Zhang, Y., Wallace, J. M., and Francis, R. C: A Pacific interdecadal climate oscillation with impacts on salmon production, Bull. Amer. Meteor. Soc., 78, 1069-1079, 1997.

Meehl, G. A., Covey, C., Delworth, T., Latif, M., McAvaney, B., Mitchell, J. F. B., Stouffer, R. J., and

Taylor, K. E.: The WCRP CMIP3 multi-model dataset: a new era in climate change research. Bull. Amer. Meteor. Soc., 88, 1383-1394, 2007.

Myneni, R. B., and co-authors: Global products of vegetation leaf area and fraction absorbed PAR from year one of MODIS data, Remote Sens. Environ., 83, 214–231, 2002.

Mori, M., Watanabe, M., Shiogama, H., Inoue, J., and Kimoto, M.: Robust Arctic sea-ice influence on the frequent Eurasian cold winters in past decades, Nature Geosci., 7, 869-873, 2014.

Marshall, A. G., Hendon, H. H., Son, S. W., and Lim, Y.: Impact of the quasi-biennial oscillation on predictability of the Madden–Julian oscillation, Clim. Dyn., doi:10.1007/s00382-016-3392-0, 2016.

McCarthy, G. D., Smeed, D. A., Johns, W. E., Frajka-Williams, E., Moat, B. I., Rayner, D., Baringer, M. O., Meinen, C. S., Collins, J., and Bryden, H. L.: Measuring the Atlantic Meridional Overturning Circulation at 26°N, Prog. Oceanogr., 130, 91-111, doi: 10.1016/j.pocean.2014.10.006, 2015.

Matsuno, T.: A dynamical mode of the stratospheric sudden warming, J. Atmos. Sci., 28, 1479-1494, 1971.

Matthes, K., and co-authors: Solar forcing for CMIP6 (v3.2), Geosc. Model Dev., 10, 2247-2302, doi:10.5194/gmd-10-2247-2017, 2017.

Meehl, G. A., Washington, W. M., Wigley, T. M. L., Arblaster, J. M., and Dai, A.: Solar and greenhouse gas forcing and climate response in the twentieth century, J. Clim., 16, 426-444, 2003.

Meehl, G. A., Arblaster, J. M., Fasullo, J. T., Hu, A., and Trenberth, K. E.: Model-based evidence of deep-ocean heat uptake during surface temperature hiatus periods, Nature Clim. Change, 1, 360-364, 2011.

Meinshausen, M., and co-authors: Historical greenhouse gas concentrations for climate modelling (CMIP6), Geosci. Model Dev., 10, 2057-2116, doi:10.5194/gmd-10-2057-2017, 2017.

Michibata, T., Suzuki, K., Sato, Y., and Takemura, T.: The sources of discrepancies in aerosol-cloud-precipitation interactions between GCM and A-Train retrievals, Atmos. Chem. Phys., 16, 15413-

Geosci. Model Dev. Discuss., https://doi.org/10.5194/gmd-2018-155
Manuscript under review for journal Geosci. Model Dev.
Discussion started: 16 July 2018

15424, 2016.

Mizuta, R.: Intensification of extratropical cyclones associated with the polar jet change in the CMIP5 global warming projections, Geophys. Res. Lett., 39, doi:10.1029/2012GL053032, 2012.

Mochizuki, M., and co-authors: Pacific decadal oscillation hindcasts relevant to near-term climate prediction, Proc. Natl. Acad. Sci. U.S.A., 107, 1833-1837, 2010.

Mochizuki, T., Kimoto, M., Chikamoto, Y., Mori, M., Watanabe, M., and Ishii, M.: Error sensitivity to initial climate states in Pacific decadal hindcasts, SOLA, 10, 39-44, 2014.

Mochizuki, T., Kimoto, M., Watanabe, M., Chikamoto, Y., and Ishii, M.: Interbasin effects of the Indian Ocean on Pacific decadal climate change, Geophys. Res. Lett., 43, 7168-7175, 2016.

Morice, C. P., Kennedy, J. J., Rayner, N. A., and Jones, P. D.: Quantifying uncertainties in global and regional temperature change using an ensemble of observational estimates: The HadCRUT4 dataset, J. Geophys. Res., doi:10.1029/2011JD017187, 2012.

Murphy, J. M.: Assessment of the practical utility of extended range ensemble forecasts, Q. J. R. Meteorol. Soc., 116, 89–125, 1990.

Murray, R. J.: Explicit generation of orthogonal grids for ocean models, J. Comput. Phys., 126, 251–273, 1996.

Nakamura, H.: Midwinter suppression of baroclinic wave activity in the Pacific, J. Atmos. Sci., 49, 1629–1642, 1992.

Nakamura, T., Toyoda, T., Ishikawa, Y., and Awaji, T.: Tidal mixing in the Kuril Straits and its impact on ventilation in the North Pacific Ocean, J. Oceanogr., 60, 411-423, 2004.

Nakano, H., and Suginohara, N.: Effects of bottom boundary layer parameterization on reproducing deep and bottom waters in a world ocean model, J. Phys. Oceanogr., 32, 1209–1227, 2002.

Neeling, J. D., Munnich, M., Su, H., Meyerson, J. E., and Holloway, C. E.: Tropical dying trends in global warming models and observations, Proc. Natl. Acad. Sci. U.S.A., 103, 6110-6115, 2006.

Geosci. Model Dev. Discuss., https://doi.org/10.5194/gmd-2018-155
Manuscript under review for journal Geosci. Model Dev.
Discussion started: 16 July 2018

Ngo-Duc, T., Oki, T., and Kanae, S.: A variable streamflow velocity method for global river routing model: model description and preliminary results, Hydrol. Earth Syst. Sci. Discuss., 4, 4389-4414, doi:10.5194/hessd-4-4389-2007, 2007.

Ninomiya, K., and Akiyama, T.: Multi-scale features of Baiu, the summer monsoon over Japan and East Asia, J. Meteor. Res. Japan, 70, 467–495, 1992.

Nitta, T., Yoshimura, K., and Abe-Ouchi, A.: Impact of arctic wetlands on the climate system: Model sensitivity simulations with the MIROC5 AGCM and a snow-fed wetland scheme, J. Hydrometeor., 18, 2923-2936, 2017.

Nitta, T., Yoshimura, K., Takata, K., O'ishi, R., Sueyoshi, T., Kanae, S., Oki, T., Abe-Ouchi, A., and Liston, G. E.: Representing variability in subgrid snow cover and snow depth in a global land model, J. Clim., 27, 3318-3330, doi:10.1175/JCLI-D-13-003, 2014.

Nozawa, T., Nagashima, T., Shiogama, H., and Crooks, S.A.: Detecting natural influence on surface air temperature change in the early twentieth century, Geophys. Res. Lett., 32, doi:10.1029/2005GL023540, 2005.

Numaguti, A., Takahashi, M., Nakajima, T., and Sumi, A.: Description of CCSR/NIES atmospheric general circulation model. National Institute for Environmental Studies, Center for Global Environmental Research Supercomputer Monograph Rep., 3, 1-48, 1997.

Olbers, D., Borowski, D., Volker, C., and Wolff, J.-O.: The dynamical balance, transport and circulation of the Antarctic Circumpolar Current. Antarctic Sci., 14, 439-470, 2004.

Oki, T. and Sud, Y.C.: Design of Total Runoff Integrating Pathways (TRIP) - A global river channel netwerk, Earth Interact., 2, 1-37, 1998.

Ono, J., Tatebe, H., Komuro, Y., Nodzu, M. I., and Ishii, M.: Mechanisms influencing seasonal to inter-annual prediction skill of sea ice extent in the Arctic Ocean in MIROC, The Cryosphere, 12, 675-683, 2018.

Geosci. Model Dev. Discuss., https://doi.org/10.5194/gmd-2018-155
Manuscript under review for journal Geosci. Model Dev.
Discussion started: 16 July 2018

Osprey, S. M., Gray, L. J., Hardiman, S. C., Butchart, N., and Hinton, T. J.: Stratospheric variability in twentieth-century CMIP5 simulations of the Met Office climate model: High top versus low top, J. Clim., 26, 1595-1606, 2013.

Park, S. and Bretherton, C. S.: The University of Washington shallow convection and moist turbulence schemes and their impact on climate simulations with the Community Atmosphere Model, J. Clim., 22, 3449-3469, 2009.

Power, S., Casey, T., Folland, C., Colman, A., and Mehta, V.: Interdecadal modulation of the impact of ENSO on Australia, Clim. Dyn., 15, 319-324, 1999.

Prather, M. J.: Numerical advection by conservation of second-order moments, J. Geophys. Res. 91, 6671–6681, 1986.

Ramankutty, N. and Foley, J.A.: Estimating historical changes in global land cover: croplands from 1700 to 1992, Global Biogeochem. Cycles, 13, 997-1027, 1999.

Rockström, J., and co-authors: A safe operating space for humanity, Nature, 461, 472-475, 2009.

Riebesell, U., Körtzinger, A., and Oschlies, A.: Sensitivities of marine carbon fluxes to ocean change, Proc. Natl. Acad. Sci. U.S.A., 106, 20602–20609, 2009.

Roberts, M. J., Clayton, A., Demory, M.-E., Donners, J., Vidale, P. L., Norton, W., Shaffrey, L., Stevens, D. P., Stevens, I., Wood, R. A., and Slingo, J.: Impact of resolution on the tropical Pacific circulation in a matrix of coupled models. J. Clim., 22, 2541–2556, 2009.

Röske, F.: A global heat and freshwater forcing dataset for ocean models, Ocean Modell., 11, 235-297, 2006.

Rossow, W. B., Walker, A. W., Beuschel, D., and Roiter, M.: International Satellite Cloud Climatology Project (ISCCP) documentation of new cloud datasets, World Climate Research Programme (ICSU and WMO), WMO/TD 737, 115pp, 1996.

Scaife, A. A., and co-authors: Climate change projections and stratosphere-troposphere interaction,

Geosci. Model Dev. Discuss., https://doi.org/10.5194/gmd-2018-155
Manuscript under review for journal Geosci. Model Dev.
Discussion started: 16 July 2018

Clim. Dyn., 38, 2089-2097, 2012.

Scaife, A. A., and co-authors: Skillful long-range predictions of European and North American winters, Geophys. Res. Lett., 41, 2514-2519, 2014.

Saji, N. H., Goswami, B. N., Vinayachandran, P. N., and Yamagata, T.: A dipole mode in the tropical Indian Ocean, Nature, 401, 360–363, 1999.

Sakamoto, T., and co-authors: MIROC4h - A new high-resolution atmosphere-ocean coupled general circulation model, J. Meteor. Soc. Jpn., 90A, 325-359, 2012.

Satoh, M., and co-authors: The non-hydrostatic icosahedral atmospheric model: description and development, Prog. Earth Planet Sci., 1:18, doi:10.1186/s40645-017-014-0018-1, 2014.

Schlesinger, M. E. and Ramankutty, N.: An oscillation in the global climate system of period 65-70 years, Nature, 376, 723－726, 1994.

Sekiguchi, M. and Nakajima, T.: A k-distribution-based radiation code and its computational optimization for an atmospheric general circulation model, J. Quant. Spectrosc. Radiat. Transfer, doi:10.1016/j.jqsrt.2008.07.13, 2008.

Sellers, P.J., and co-authors: The ISLSCP Initiative I global datasets: surface boundary conditions and atmospheric forcings for land-atmosphere studies, Bull. Amer. Meteor. Soc., 1987-2005, 1997.

Shaffrey, L., and co-authors: U.K. HiGEM: The new U.K. high resolution global environment model - Model description and basic evaluation, J. Clim., 22, 1861–1896, 2009.

Shiogama, H., Watanabe, M., Yoshimori, M., Yokohata, T., Ogura, T., Annan, J.D., Hargreaves, J.C., Abe, M., Kamae, Y., O'ishi, R., Nobui, R., Emori, S., Nozawa, T., Abe-Ouchi, A., and Kimoto, M.: Perturbed physics ensemble using the MIROC5 coupled atmosphere-ocean GCM without flux corrections: experimental design and results, Clim. Dyn., 39, 3041-3056, 2012.

Shiogama, H., Watanabe, M., Imada, Y., Mori, M., Kamae, Y., Ishii, M., and Kimoto, M.: Attribution of the June-July 2013 heat wave in the southwestern United States, SOLA, 10, 122-126, 2014.

Geosci. Model Dev. Discuss., https://doi.org/10.5194/gmd-2018-155
Manuscript under review for journal Geosci. Model Dev.
Discussion started: 16 July 2018

Geoscientific Model Development Discussions
Open Access EGU

Sillmann, J., Kharin, V. V., Zwiers, F. W., Zhang, X., and Bronaugh, D.: Climate extremes indices in the CMIP5 multimodel ensemble: Part 2. Future climate projections, J. Geophys. Res., 118, 2473-2493, 2013.

Steele, M., Morley, R., and Ermold, W.: PHC: A global ocean hydrography with a high-quality Arctic Ocean, J. Clim., 14, 2079-2087, 2001.

Stott, P. A., Stone, D. A. and Allen, M. R.: Human contribution to the European heatwave of 2003, Nature, 432, 610-614, 2004.

Sudo, K., Takahashi, M., Kurokawa, J., and Akimoto, H.: CHASER: A global chemical model of the troposphere 1. Model description, J. Geophys. Res., 107, 4339, doi:10.1029/2001JD001113, 2002.

Suzuki, K., Golaz, J-.C, and Stephens, G. L., 2013: Evaluating cloud tuning in a climate model with satellite observations, Geophys. Res. Lett., 40, 4464-4468, 2013.

Suzuki, T., Saito, F., Nishimura, T., and Ogochi, K.: Heat and freshwater exchanges between sub-models of MIROC version 4, JAMSTEC Rep. Res. Dev., 9, 2009 (in Japanese).

Suzuki, T., Hasumi, H., Sakamoto, T. T., Nishimura, T., Abe-Ouchi, A., Segawa, T., Okada, N., Oka, A., and Emori, S.: Projection of future sea level and its variability in a high-resolution climate model: ocean processes and Greenland and Antarctic ice-melt contributions, Geophys. Res. Lett., 32, doi:10.1029/2005GL023677, 2005.

Suzuki, T. and Ishii, M.: Regional distribution of sea level changes resulting from enhanced greenhouse warming in the Model for Interdisciplinary Research on Climate version 3.2, Geophys. Res. Lett., 38, doi:10.1029/2010GL045693, 2011.

Takata, K., Emori, S., and Watanabe, T.: Development of the Minimal Advanced Treatments of Surface Interraction and RunOff (MATSIRO), Global and Planetary Change, 38, 209-222, 2003.

Takemura, T., Okamoto, H., Maruyama, Y., Numaguti, A., Higurashi, A., and Nakajima, T.: Global three-dimensional simulation of aerosol optical thickness distribution of various origins, J. Geophys.

Geosci. Model Dev. Discuss., https://doi.org/10.5194/gmd-2018-155
Manuscript under review for journal Geosci. Model Dev.
Discussion started: 16 July 2018

Res., 105, 17853-17873, 2000.

Takemura, T., Nakajima, T., Dubovik, O., Holben, B. N., and Kinne, S.: Single-scattering albedo and radiative forcing of various aerosol species with a global three-dimensional model, J. Clim., 15, 333-352, 2002.

Takemura, T., Nozawa, T., Emori, S., Nakajima, T. Y., and Nakajima, T.: Simulation of climate response to aerosol direct and indirect effects with aerosol transport-radiation model, J. Geophys. Res., 110, D02202, doi:10.1029/2004JD005029, 2005.

Takemura, T., Egashira, M., Matsuzawa, K., Ichijo, H., O'ishi, R., and Abe-Ouchi, A.: A simulation of the global distribution and radiative forcing of soil dust aerosols at the Last Glacial Maximum, Atmos. Chem. Phys., 9, 3061-3073, doi:10.5194/acp-9-3061-2009, 2009.

Talley, L. D., Reid, J. L., and Robbins, P. E.: Date-based meridional overturning streamfuctions for the global ocean, J. Clim., 16, 3213-3226, 2003.

Tatebe, H. and Yasuda, I: Oyashio southward intrusion and cross-gyre transport related to diapycnal upwelling in the Okhotsk Sea, J. Phys. Oceanogr., 34, 2327-2341, 2004.

Tatebe, H. and Hasumi, H.: Formation mechanism of the Pacific equatorial thermocline revealed by a general circulation model with a high accuracy tracer advection scheme, Ocean Modell., 35, 245-252, 2010.

Tatebe, H., and co-authors: The initialization of the MIROC climate models with hydrographic data assimilation for decadal prediction, J. Meteor. Soc. Jpn., 90A, 275-294, 2012.

Tatebe, H., Imada, Y., Mori, M., Kimoto, M., and Hasumi, H.: Control of decadal and bidecadal climate variability in the tropical Pacific by the off-equatorial South Pacific Ocean, J. Clim., 26, 6524-6534, 2013.

Taucher, J. and Oschlies, A.: Can we predict the direction of marine primary production change under global warming? Geophys. Res. Lett., 38, doi:10.1029/2010GL045934, 2011.

Geosci. Model Dev. Discuss., https://doi.org/10.5194/gmd-2018-155
Manuscript under review for journal Geosci. Model Dev.
Discussion started: 16 July 2018

Taylor, K. E., Stouffer, R. J., and Meehl, G. A.: A summary of the CMIP5 experiment design. https://pcmdi.llnl.gov/?cmip5/docs/Taylor_CMIP5_22Jan11_marked.pdf, 2011.

Thompson, D. M., Cole, J. E., Shen, G. T., Tudhope, A. W., and Meehl, G. A.: Early twentieth-century warming linked to tropical Pacific wind strength. Nature Geosci., 8, doi:10.1038/ngeo2321, 2014.

Thomason, L., Vernier, J.-P., Bourassa, A., Arfeuille, F., Bingen, C., Peter, T., and Luo, B.: Stratospheric Aerosol Data Set (SADS Version 2) Prospectus, to be submitted to Geosci. Model Dev. Dis-cuss., 2016.

Trenberth, K. E., and Shea, D. J.: Atlantic hurricanes and natural variability in 2005, Geophys. Res. Lett., 33, L12704, doi:10.1029/2006GL026894, 2006.

van Marle, M.J.E., and co-authors: Historic global biomass burning emissions for CMIP6 (BB4CMIP) based on merging satellite observations with proxies and fire models (1750-2015), Geosci. Model Dev., 10, 3329-3357, doi:10.5194/gmd-10-3329-2017, 2017.

Waliser, D. E., Li, J.-L. F., L'Ecuyer, T. S., and Chen, W.-T.: The impact of precipitating ice and snow on the radiation balance in global climate models, Geophys. Res. Lett., 38, L06802, doi:10.1029/2010GL046478, 2011.

Wallace, J. M. and Gutzler, D. S.: Teleconnections in the geopotential height field during the northern hemisphere winter, Mon. Wea. Rev., 109, 784-812, 1981.

Watanabe, M., Suzuki, T., O'ishi, R., Komuro, Y., Watanabe, S., Emori, S., Takemura, T., Chikira, M., Ogura, T., Sekiguchi, M., Takata, K., Yamazaki, D., Yokohata, T., Nozawa, T., Hasumi, H., Tatebe, H., and M. Kimoto, M.: Improved climate simulation by MIROC5: Mean states, variability, and climate sensitivity, J. Clim., 23, 6312-6335, DOI: 10.1175/2010JCLI3679.1, 2010.

Watanabe, M., Shiogama, H., Tatebe, H., Hayashi, M., Ishii, M., and Kimoto, M.: Contribution of natural decadal variability to global warming acceleration and hiatus, Nature Clim. Change, 4, 893-897, 2014.

Geosci. Model Dev. Discuss., https://doi.org/10.5194/gmd-2018-155
Manuscript under review for journal Geosci. Model Dev.
Discussion started: 16 July 2018

Watanabe, M., Shiogama, H., Imada, Y., Mori, M., Ishii, M., and Kimoto, M.: Event attribution of the August 2010 Russian heat wave, SOLA, 9, 65-68, 2013.

Watanabe, S., Hajima, T., Sudo, K., Nagashima, T., Takemura, T., Okajima, H., Nozawa, T., Kawase, H., Abe, M., Yokohata, T., Ise, T., Sato, H., Kato, E., Takata, K., Emori, S., and Kawamiya, M.: MIROC-ESM 2010: model description and basic results of CMIP5-20c3m experiments, Geosci. Model Dev., 4, 845-872, doi:10.5194/gmd-4-845-2011, 2011.

Watanabe, M., and Kawamiya, M.: Remote effects of mixed layer development on ocean acidification in the subsurface layers of the North Pacific, J. Oceanogr., 73, 771-784, 2017.

Wood, R. and Bretherton, C. S.: On the relationship between stratiform low cloud cover and lower-tropospheric stability, J. Clim., 19, 6425-6432, 2006.

Webster, P. J., Moore, A. M., Loschnigg, J. P., and Leben, R. R.: Coupled ocean-atmosphere dynamics in the Indian Ocean during 1997-98, Nature, 401, 35-360, 1999.

Wheeler, M. and Kiladis, G. N.: Convectively coupled equatorial waves: Analysis of clouds and temperature in the wavenumberfrequency domain, J. Atmos. Sci., 56, 374-399, 1999.

Yamazaki, D., Oki, T., and Kanae, S.: Deriving a global river network map and its sub-grid topographic characteristics from a fine-resolution flow direction map, Hydrol. Earth Syst. Sci., 13, 2241–2251, 2009.

Yang, P., Lei, B., Baum, B.A., Liou, K-N., Kattawar, G.W., Mischenko, M. I., and Cole, B.: Spectrally consistent scattering, absorption, and polarization properties of atmospheric ice crystals at wavelengths from 0.2 to 100 μm, J. Atm. Sci., 70, 330-347, 2013.

Yoo, C. and Son, S. W.: Modulation of the boreal wintertime Madden Julian oscillation by the stratospheric quasi-biennial oscillation, Geophys. Res. Lett., 43, 1392-1398, 2016.

Zappa, G., Shaffrey, L. C., Hodges, K. I., Sansom, P. G., and Stephenson, D. B.: A multi-model assessment of future projections of North Atlantic and European extratropical cyclones in the CMIP5

Geosci. Model Dev. Discuss., https://doi.org/10.5194/gmd-2018-155
Manuscript under review for journal Geosci. Model Dev.
Discussion started: 16 July 2018

climate models, J. Clim., doi:10.1175/JCLI-D-12-00573.1, 2013.

Zhang, X. B., and co-authors: Detection of human influence on twentieth-century precipitation trends, Nature, 448, 461-464, 2007.

Zhang, Y., Sperber, K. R., and Boyle, J. S.: Climatology and interannual variation of the East Asian winter monsoon: Results from the 1979-95 NCEP/NCAR reanalysis, Mon. Wea. Rev., 125, 2605-2619, 1997.

Zhang, Y., Rossow, W. B., Lacis, A. A., Oinas, V., and Mishchenko, M. I.: Calculation of radiative fluxes from the surface to top of atmosphere based on ISCCP and other global data sets: Refinements of the radiative transfer model and the input data, J. Geophys. Res., 109, doi:10.1029/2003JD004457, 2004.

Geosci. Model Dev. Discuss., https://doi.org/10.5194/gmd-2018-155
Manuscript under review for journal Geosci. Model Dev.
Discussion started: 16 July 2018

Geoscientific Model Development
Discussions
Open Access

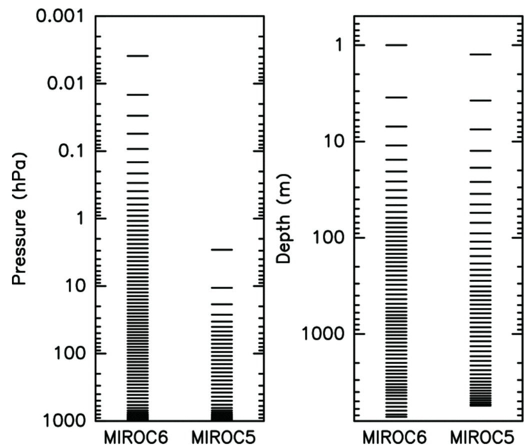

Fig. 1. Vertical levels for the atmospheric (left panel) and the oceanic (right panel) components of MIROC6 and MIROC5.

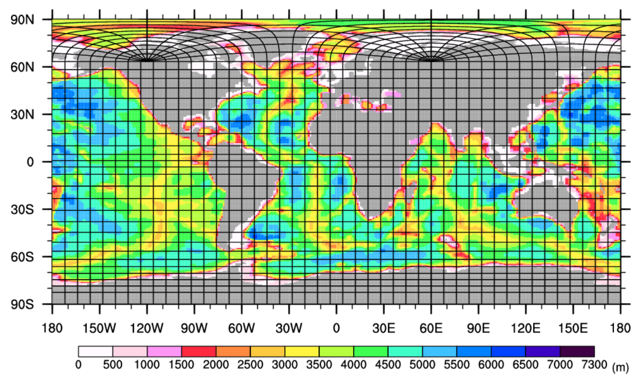

Fig. 2. Horizontal grid coordinate system and model bathymetry of the ocean component of MIROC6.

Geosci. Model Dev. Discuss., https://doi.org/10.5194/gmd-2018-155
Manuscript under review for journal Geosci. Model Dev.
Discussion started: 16 July 2018

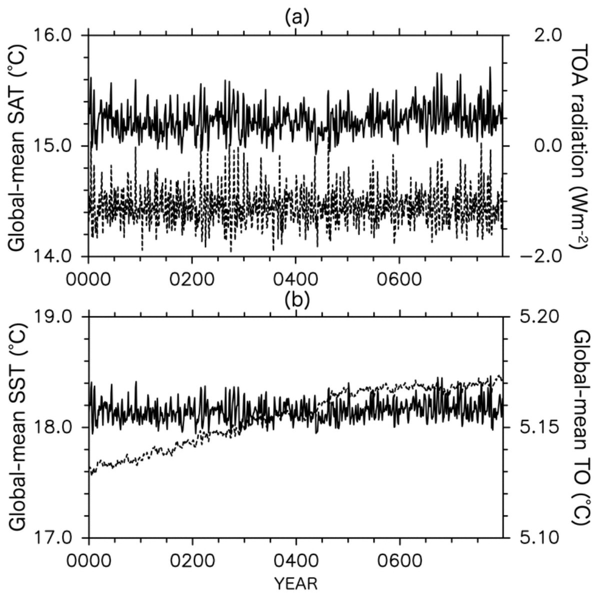

Fig. 3. (a) Time series of the global-mean SAT (solid) and the TOA radiation budget (dashed; upward positive). (b) Same as (a), but for the global-mean SST (solid) and the ocean temperature through the full water column (dashed).

Geosci. Model Dev. Discuss., https://doi.org/10.5194/gmd-2018-155
Manuscript under review for journal Geosci. Model Dev.
Discussion started: 16 July 2018

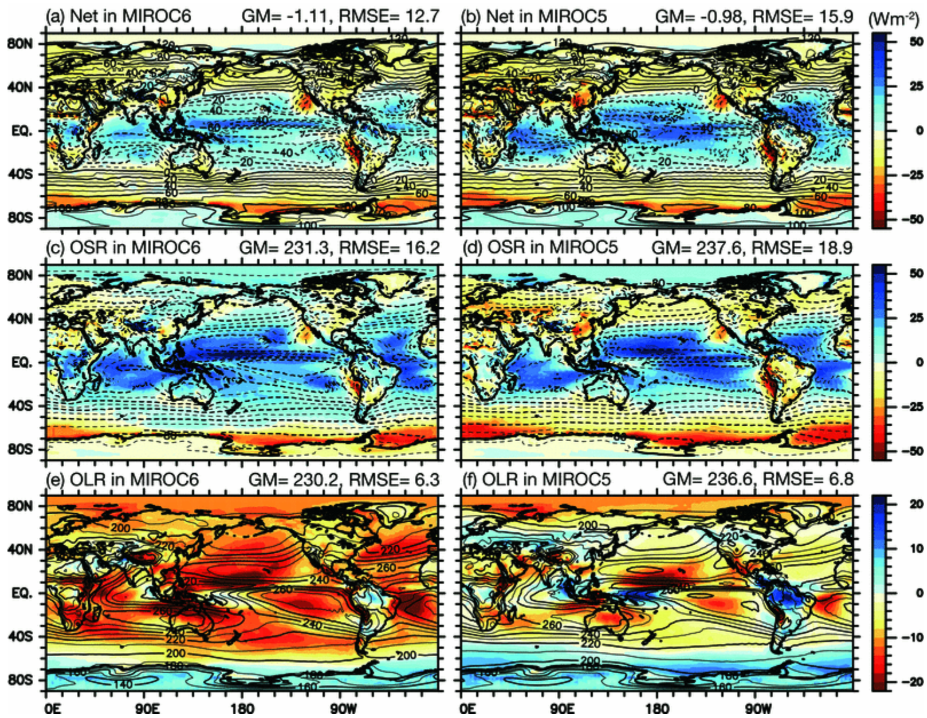

Fig. 4. Annual-mean TOA radiative fluxes in MIROC6 (left panels) and MIROC5 (right panels). Upward is defined as positive. The net, outgoing shortwave, and outgoing longwave radiations are aligned from the top to the bottom. Colors indicate errors with respect to observations (CERES) and contours denote values in each model. The global-mean values and root-mean-squared errors are indicated by GM and RMSE, respectively. Note that a different color scale is used for the longwave radiations.

Geosci. Model Dev. Discuss., https://doi.org/10.5194/gmd-2018-155
Manuscript under review for journal Geosci. Model Dev.
Discussion started: 16 July 2018

Geoscientific Model Development Discussions
Open Access

1517

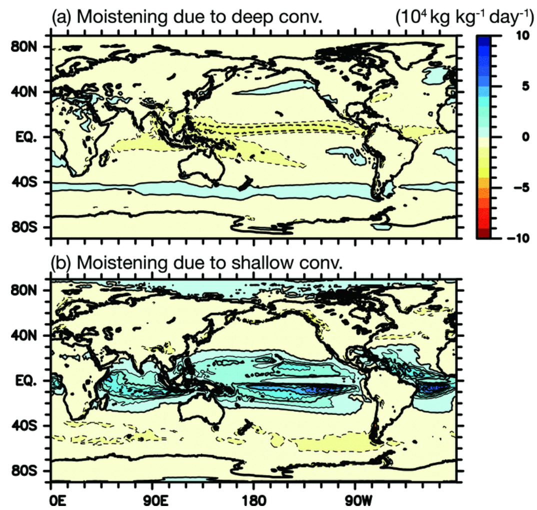

1518

1519 Fig. 5. Annual-mean moistening rate associated with (a) deep convections and (b) shallow convections

1520 in MIROC6 at the 850 hPa pressure level.

1521

Geosci. Model Dev. Discuss., https://doi.org/10.5194/gmd-2018-155
Manuscript under review for journal Geosci. Model Dev.
Discussion started: 16 July 2018

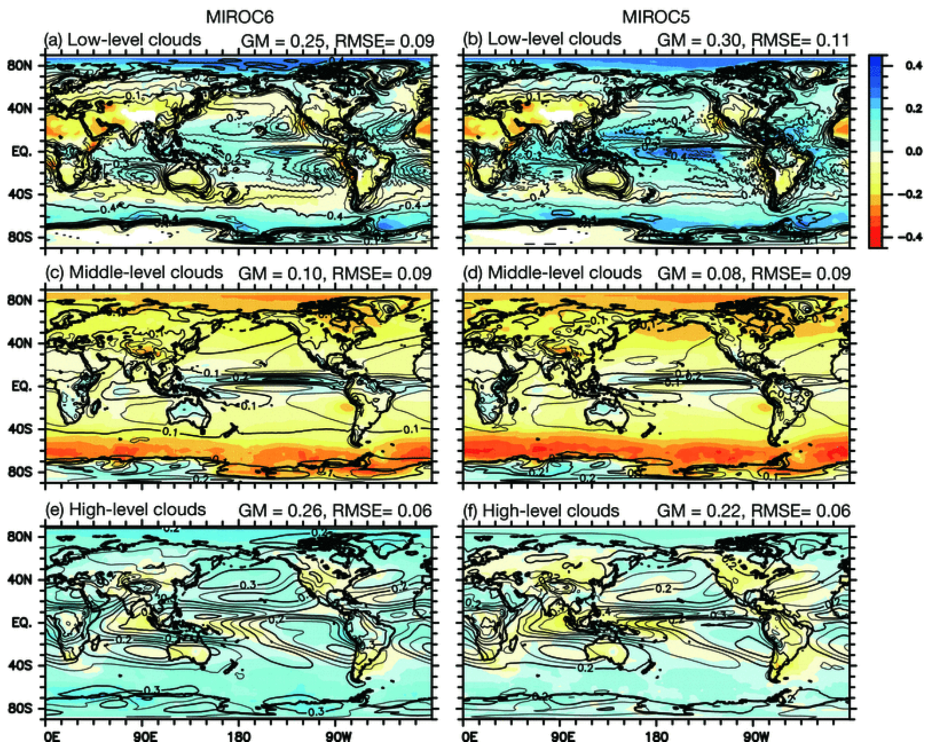

Fig. 6. Same as Fig. 4, but for cloud covers in MIROC6 (left panels) and MIROC5 (right panels). Low-, middle-, and high-level cloud covers are aligned from the top to the bottom. The tops for low-, middle-, and high-level clouds are defined to exist below the 680 hPa, between the 680 hPa and 440 hPa, and above the 440 hPa pressure levels, respectively. The unit is non-dimensional. ISCCP climatology is used as observations.

Geosci. Model Dev. Discuss., https://doi.org/10.5194/gmd-2018-155
Manuscript under review for journal Geosci. Model Dev.
Discussion started: 16 July 2018

Geoscientific Model Development Discussions
Open Access

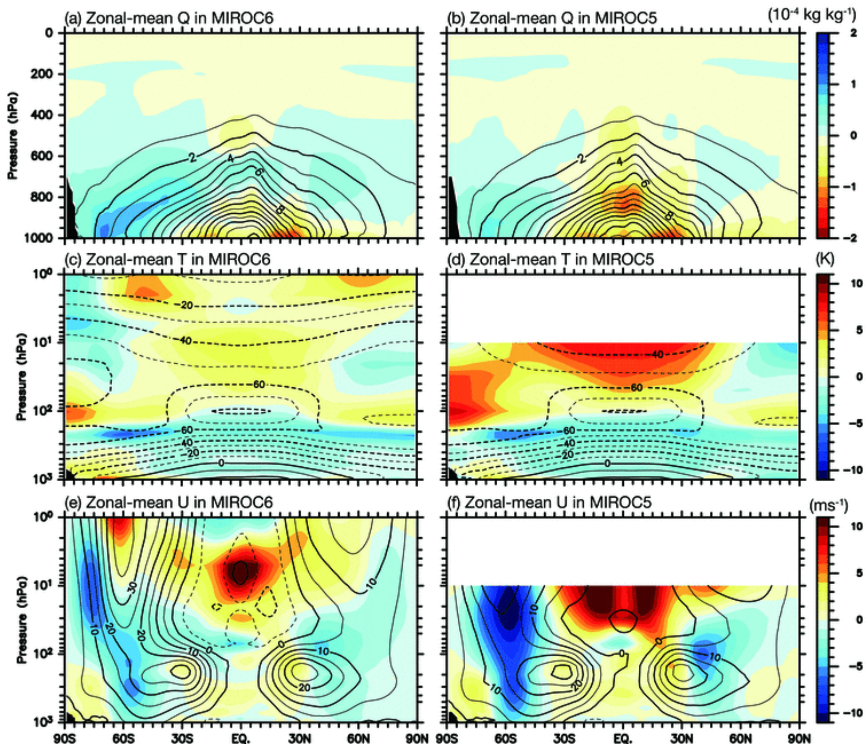

Fig. 7. Annual and zonal-mean specific humidity (top panels), temperature (middle), and zonal wind (bottom) in MIROC6 (left) and MIROC5 (right). Colors indicate errors with respect to observations (ERA-I) and contours denote values in each model.

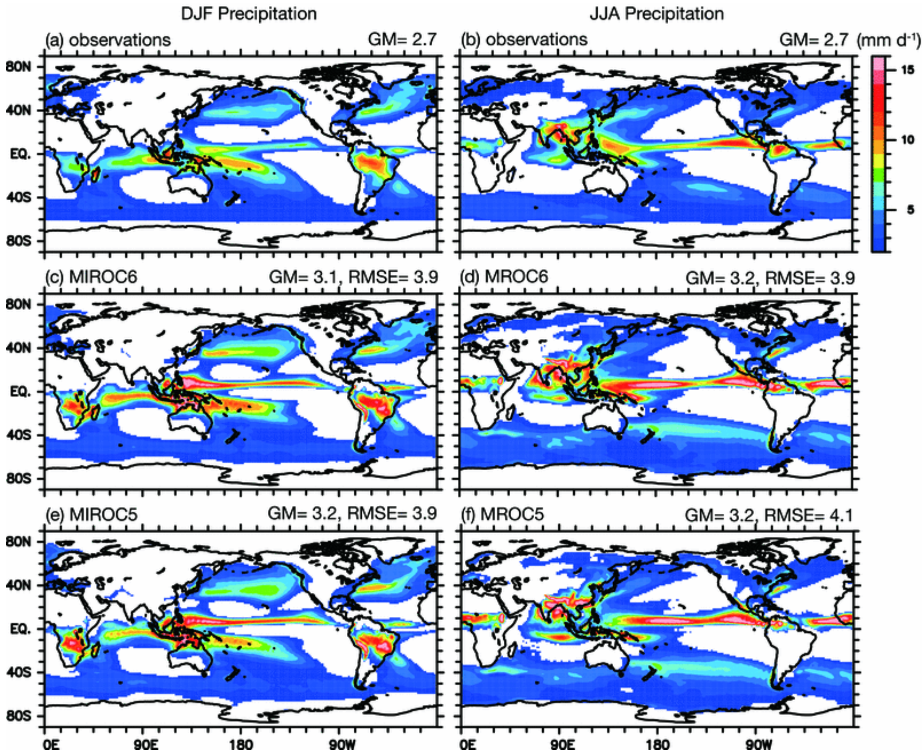

Fig. 8. Precipitation in boreal winter (December–February; left panels) and summer (June–August; right panels) in observations (top; GPCP), MIROC6 (middle), and MIROC5 (bottom). Areas with precipitation smaller than 3 mm d^{-1} are not colored.

Geosci. Model Dev. Discuss., https://doi.org/10.5194/gmd-2018-155
Manuscript under review for journal Geosci. Model Dev.
Discussion started: 16 July 2018

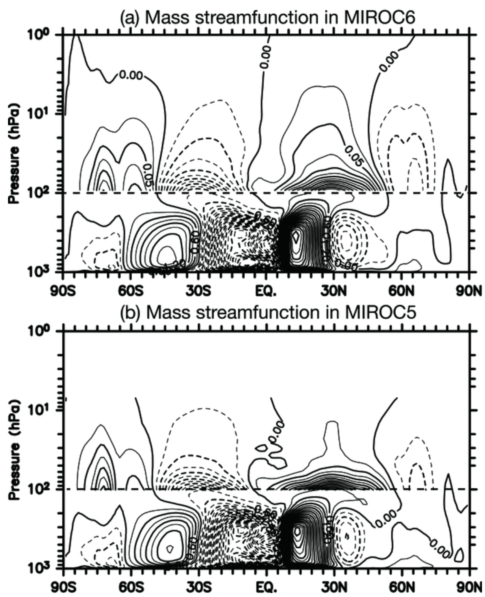

Fig. 9. Annual-mean mass stream functions in (a) MIROC6 and (b) MIROC5. Contour interval is 0.3 (0.025) × 10^{10} kg s^{-1} below (above) the 100 hPa pressure level. Negative values are denoted by dashed contours, and the horizontal dashed lines indicate the 100 hPa pressure level.

Geosci. Model Dev. Discuss., https://doi.org/10.5194/gmd-2018-155
Manuscript under review for journal Geosci. Model Dev.
Discussion started: 16 July 2018

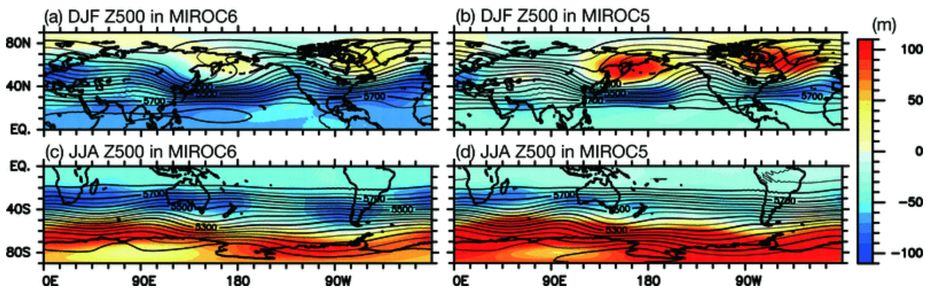

Fig. 10. Same as Fig. 4, but for the wintertime 500 hPa pressure level in MIROC6 (left panels) and MIROC5 (right panels). Maps for boreal (austral) winter are shown in the upper (lower) panels. ERA-I is used as observations.

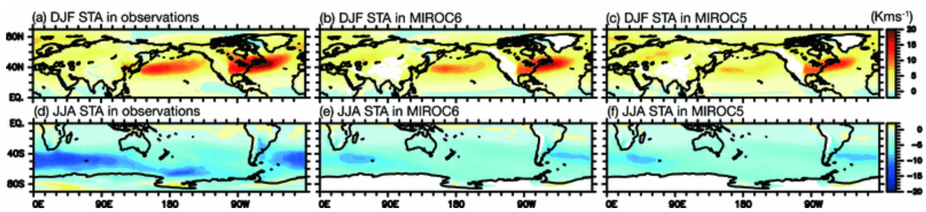

Fig. 11. Wintertime storm track activity (STA) in observations (left), MIROC6 (center), and MIROC5 (right). STA is defined as 8-day-highpass-filtered eddy meridional temperature flux at the 850 hPa pressure level. Maps for boreal (austral) winter are shown in the upper (lower) panels. ERA-I is used as observations.

Geosci. Model Dev. Discuss., https://doi.org/10.5194/gmd-2018-155
Manuscript under review for journal Geosci. Model Dev.
Discussion started: 16 July 2018

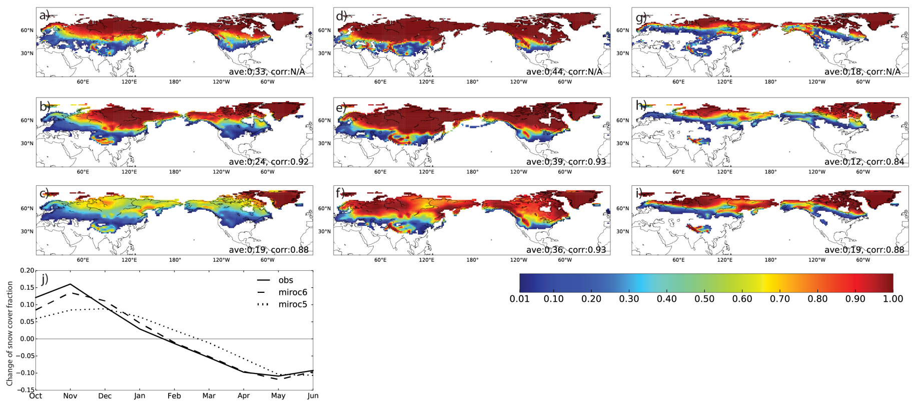

Fig. 12. Snow cover fractions for observations (top panels), MIROC6 (middle), and MIROC5 (bottom). Maps in November, February, and May are aligned from the left to the right. The unit is non-dimensional. Areas where snow cover fractions are less than 0.01 are masked. Ave and corr. in the panels indicate spatial averages and correlation coefficients between observations and models over the land surface in the Northern Hemisphere, respectively. Time series in the bottom-left panel shows temporal rate of change of the monthly spatial averages. Snow-cover dataset of the Northern Hemisphere EASE-Grid 2.0 is used as observations.

Geosci. Model Dev. Discuss., https://doi.org/10.5194/gmd-2018-155
Manuscript under review for journal Geosci. Model Dev.
Discussion started: 16 July 2018

Geoscientific Model Development Discussions

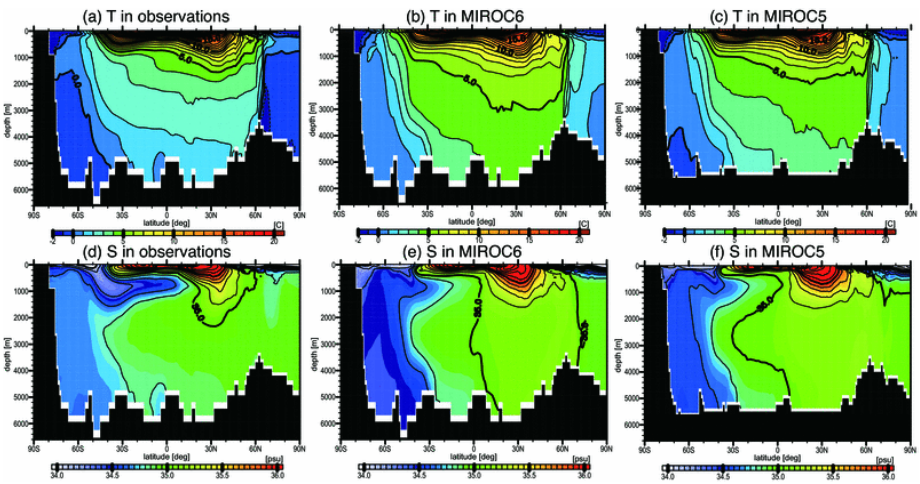

Fig. 13. Annual-mean potential temperature (upper panels; unit is °C) and salinity (lower; psu) in the Atlantic sector from observations (left), MIROC6 (middle), and MIROC5 (right). ProjD is used as observations.

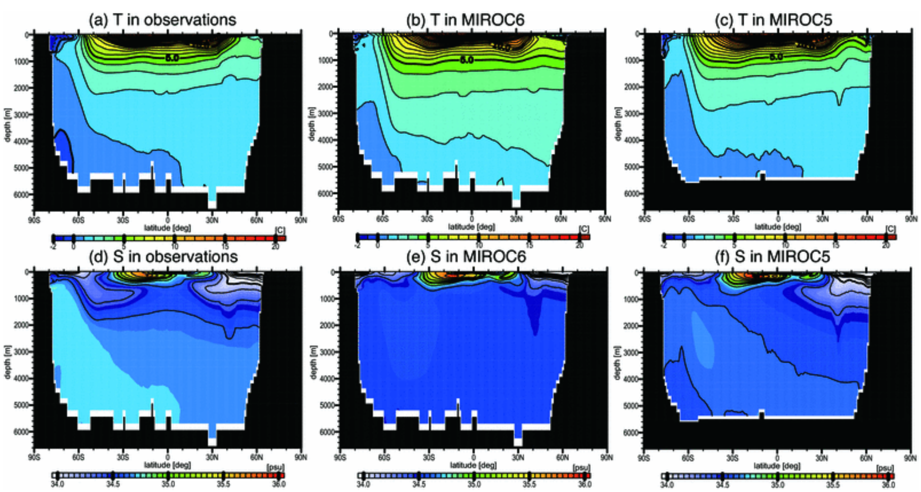

Fig. 14. Same as Fig. 13, but for the Pacific sector.

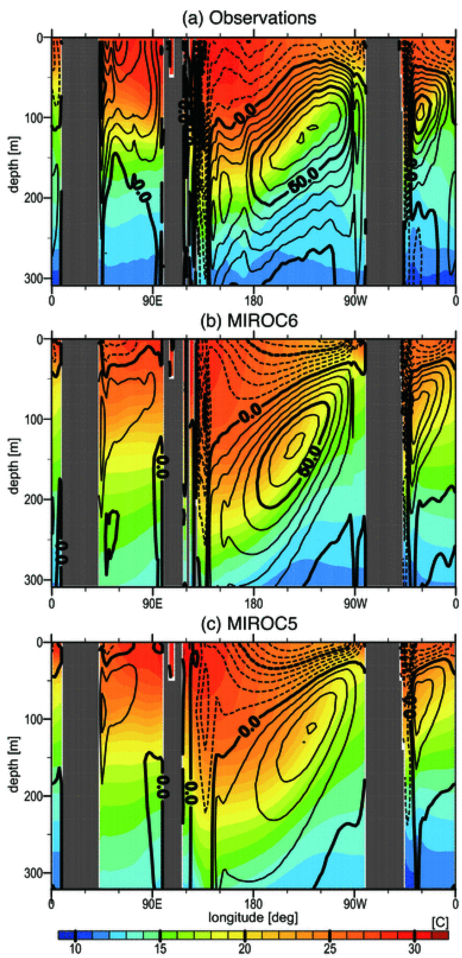

Fig. 15. Annual-mean climatology of temperature (°C; colors) and zonal current speed (cm s^{-1}; contours) along the equator (1°S–1°N) in (a) observations (ProjD and SODA), (b) MIROC6, and (c) MIROC5.

Geosci. Model Dev. Discuss., https://doi.org/10.5194/gmd-2018-155
Manuscript under review for journal Geosci. Model Dev.
Discussion started: 16 July 2018

Geoscientific Model Development Discussions
Open Access

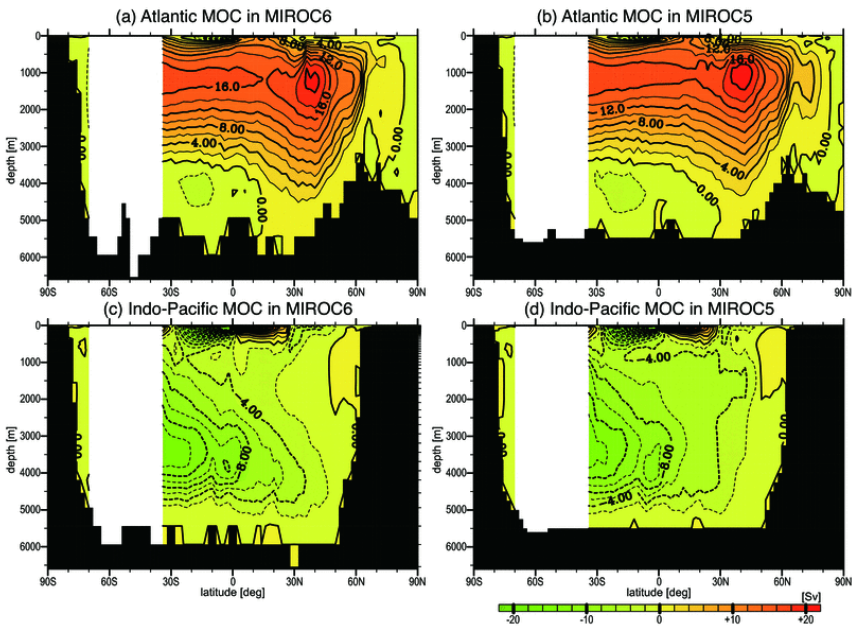

Fig. 16. Annual-mean meridional overturning circulations in the Atlantic (upper panels) and the Indo-Pacific sectors (lower) in MIROC6 (left) and MIROC5 (right). The unit is Sv ($\equiv 10^6$ m^{3}s^{-1}).

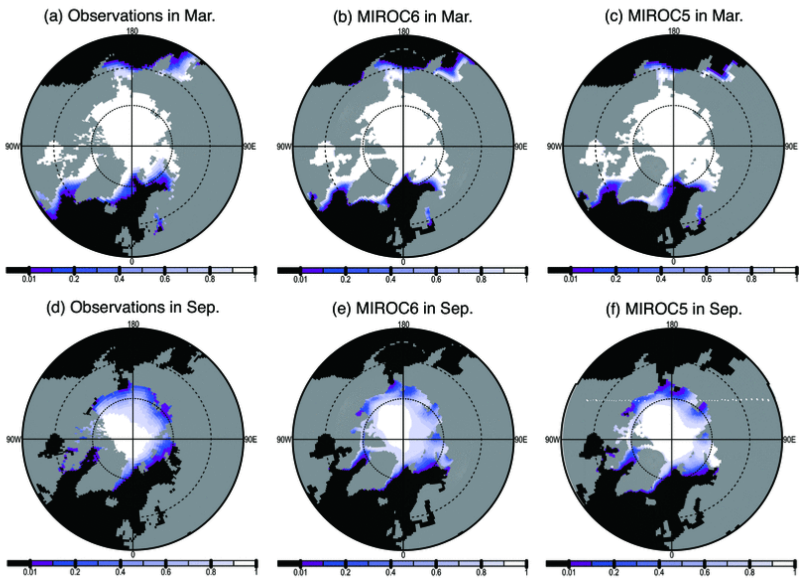

Fig. 17. Northern Hemisphere sea-ice concentrations in March (upper panels) and September (lower panels) for observations (left), MIROC6 (middle), and MIROC5 (right). The unit is non-dimensional. Satellite-based sea-ice concentration data of the SSM/I are used as observations.

Geosci. Model Dev. Discuss., https://doi.org/10.5194/gmd-2018-155
Manuscript under review for journal Geosci. Model Dev.
Discussion started: 16 July 2018

Geoscientific Model Development
Discussions
Open Access

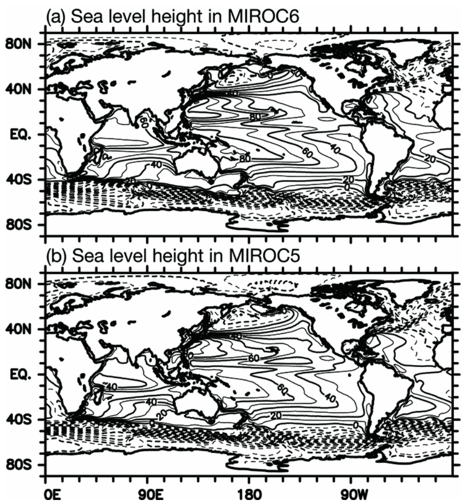

Fig. 18. Annual-mean sea level height in (a) MIROC6 and (b) MIROC5. Contour interval is 20 cm. Negative values are denoted by dashed lines. Note that loading due to sea-ice and accumulated snow on sea-ice are removed from the sea level height and that the global-mean value is also eliminated.

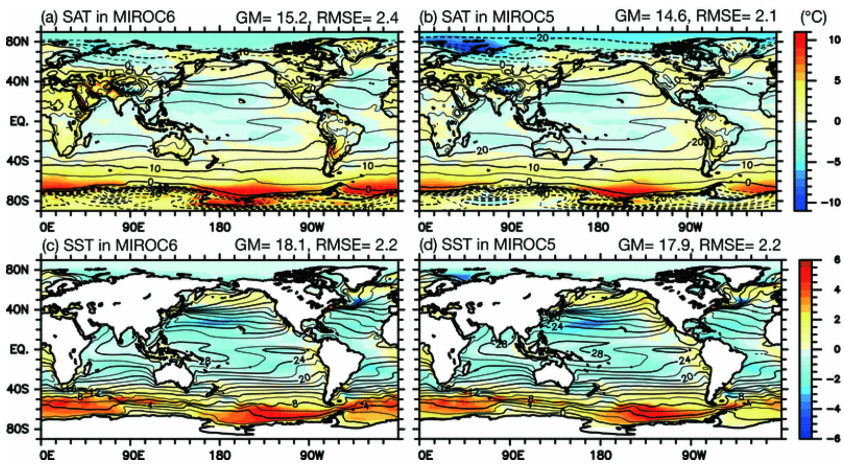

Fig. 19. Same as Fig. 4, but for annual-mean SAT (upper panels) and SST (lower panels). ERA-I for the SAT and the ProjD for the SST are used as observations.

Geosci. Model Dev. Discuss., https://doi.org/10.5194/gmd-2018-155
Manuscript under review for journal Geosci. Model Dev.
Discussion started: 16 July 2018

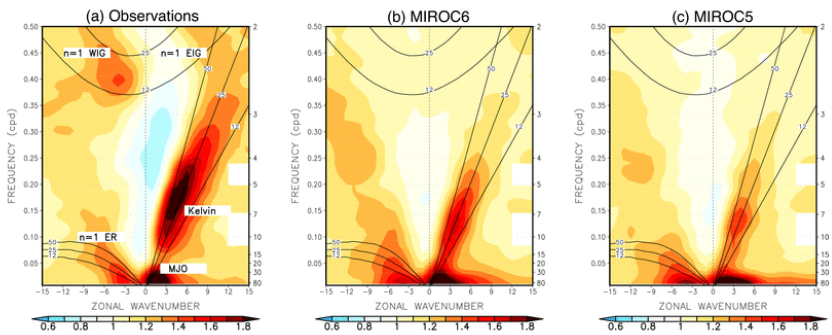

Fig. 20. Zonal wavenumber–frequency power spectra of the symmetric component of OLR divided by background power in (a) observations (NOAA OLR), (b) MIROC6, and (c) MIROC5. Dispersion curves of equatorial waves for the three equivalent depths of 12, 25, and 50 m are indicated by black lines. Signals corresponding to the westward and eastward inertio-gravity (WIG and EIG) waves, the equatorial Rossby (ER) waves, equatorial Kelvin waves, and Madden-Julian oscillation (MJO) are labeled in (a). The unit of the vertical axes is cycle per day (cpd).

Geosci. Model Dev. Discuss., https://doi.org/10.5194/gmd-2018-155
Manuscript under review for journal Geosci. Model Dev.
Discussion started: 16 July 2018

Geoscientific Model Development
Discussions

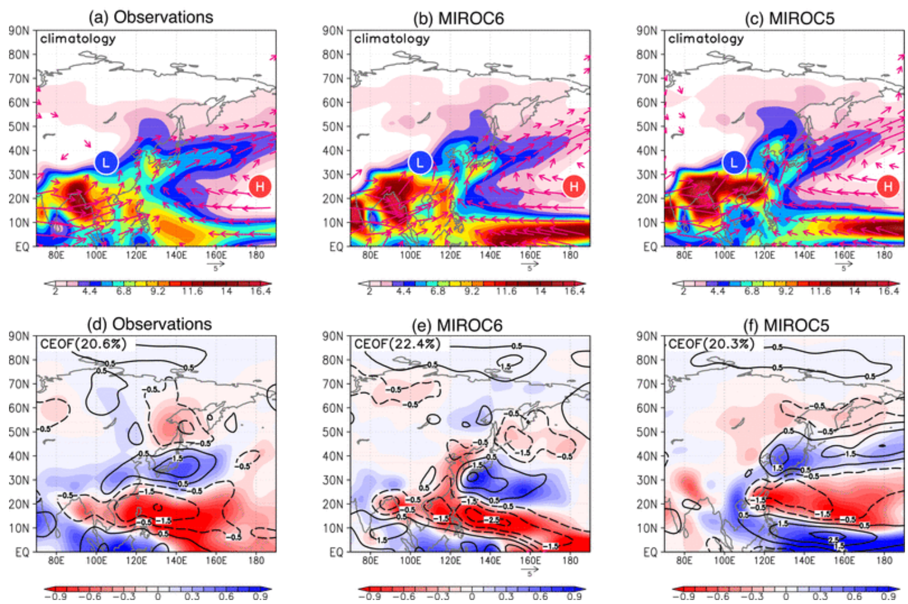

Fig. 21. (a-c) Summertime (JJA) climatology of precipitation (shading, mm day^{-1}) and the 850 hPa horizontal wind (vector; m s^{-1}) for (a) observations (ERA-I), (b) MIROC6, and (c) MIROC5. (d-f) Anomalies of summertime precipitation (shading; mm day $^{-1}$) and the 850 hPa vorticity (contour; 10^{-6} s^{-1}) regressed to the time series of EOF1 of the 850 hPa vorticity over [100°E–150°E, 0°N–60°N] for (d) observations, (e) MIROC6, and (f) MIROC5.

Geosci. Model Dev. Discuss., https://doi.org/10.5194/gmd-2018-155
Manuscript under review for journal Geosci. Model Dev.
Discussion started: 16 July 2018

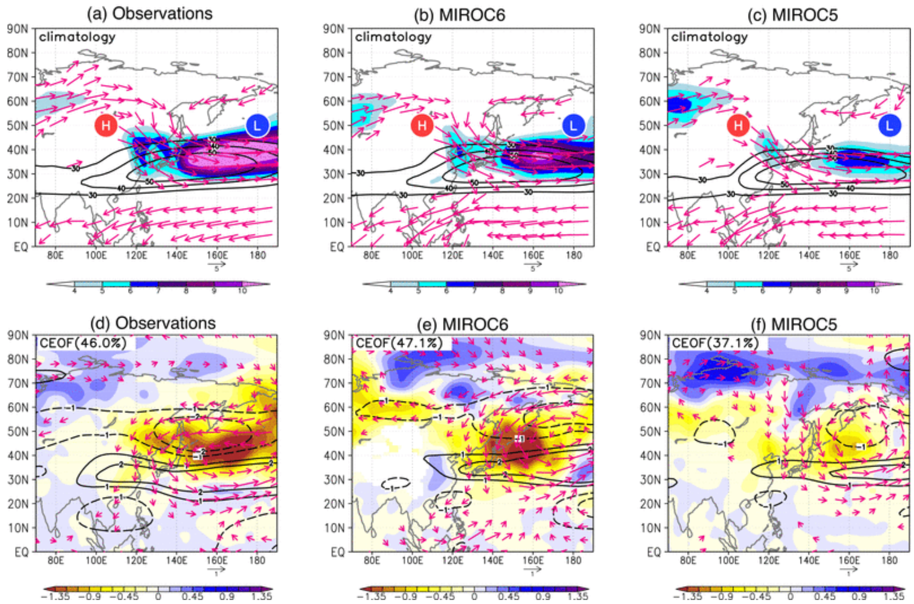

Fig. 22. (a-c) Wintertime (DJF) climatology of STA (shading; K m s^{-1}), the 300 hPa zonal wind (contour; m s^{-1}), and the 300 hPa horizontal wind (vector; m s^{-1}) for (a) observations (ERA-I), (b) MIROC6, and (c) MIROC5. (d-f) As in (a-c), but for anomalies regressed onto the time series of the EOF1 of the 850 hPa meridional wind over [120°E–150°E, 30°N–60°N].

Geosci. Model Dev. Discuss., https://doi.org/10.5194/gmd-2018-155
Manuscript under review for journal Geosci. Model Dev.
Discussion started: 16 July 2018

Geoscientific Model Development
Discussions
Open Access

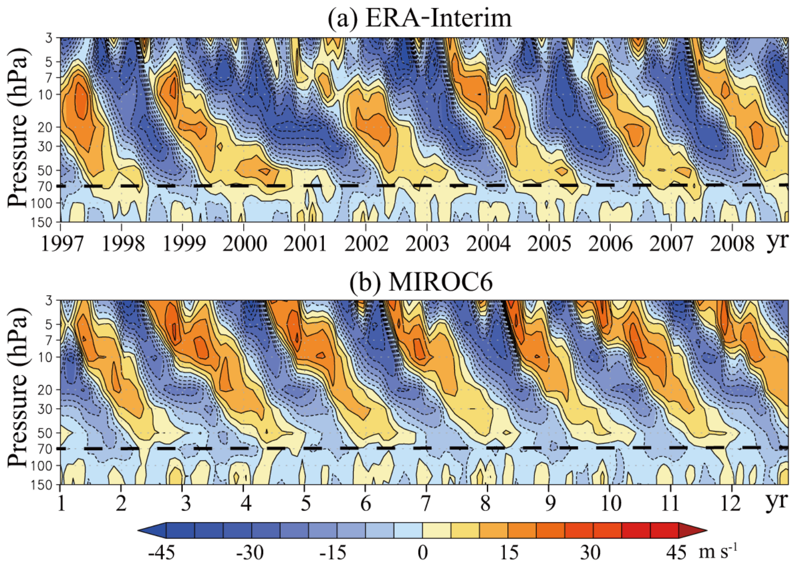

Fig. 23. Time-height cross section of the monthly mean, zonal mean zonal wind over the equator for (a) observations (ERA-I) and (b) MIROC6. The contour intervals are 5 m s^{-1}. Dashed lines correspond to the altitude of the 70 hPa pressure level. The red and blue colors correspond to westerlies and easterlies, respectively.

Geosci. Model Dev. Discuss., https://doi.org/10.5194/gmd-2018-155
Manuscript under review for journal Geosci. Model Dev.
Discussion started: 16 July 2018

Geoscientific Model Development
Open Access
Discussions

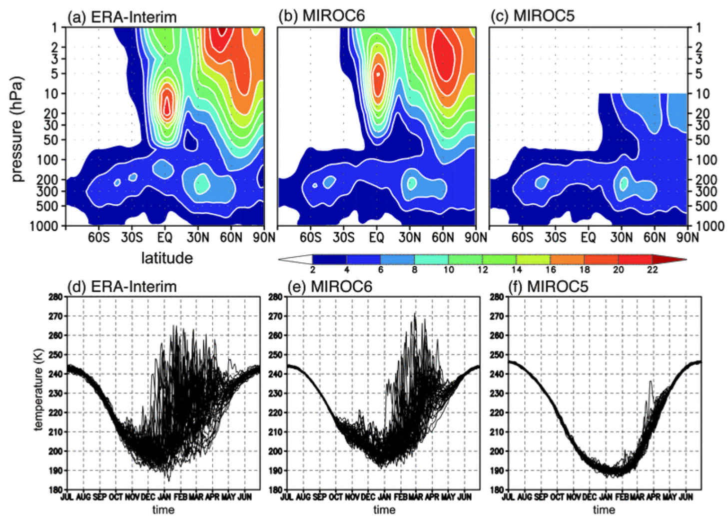

Fig. 24. (a)-(c) Standard deviation of monthly and zonal-mean zonal wind in February for (a) observations (ERA-I) in 1979–2014, (b) MIROC6, and (c) MIROC5 during 60-year period. Unit is m s^{-1}. (d-f) Daily variation of temperature at the 10 hPa pressure level on the North Pole for (d) observations (ERA-I), (e) MIROC6, and (f) MIROC5. Daily mean data during 36-year period are included in each panel (1979–2014 for observations).

Geosci. Model Dev. Discuss., https://doi.org/10.5194/gmd-2018-155
Manuscript under review for journal Geosci. Model Dev.
Discussion started: 16 July 2018

Geoscientific Model Development Discussions
Open Access

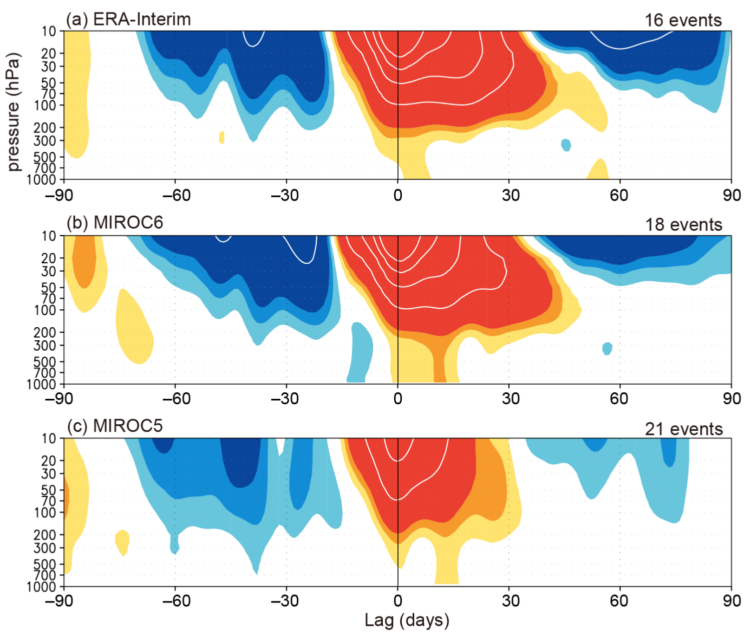

Fig. 25. Composites of time development of the zonal-mean NAM index for stratospheric weak polar vortex events in (a) observations (ERA-I), (b) MIROC6, and (c) MIROC5. The indices having dimension of geopotential height (m), and red colors denote negative values. Interval of colors (contours) is 50 (400) m. The number of events included in the composite are indicated above each panel.

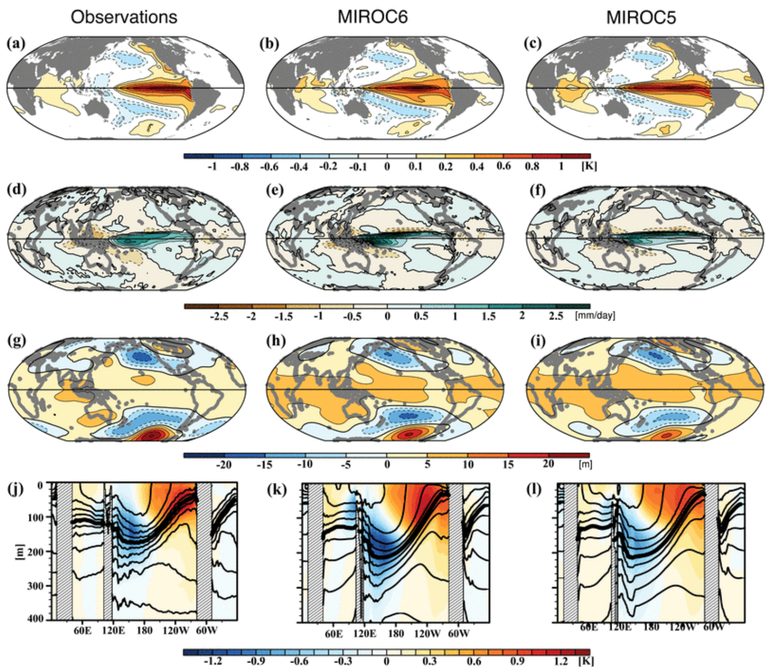

Figure 26. Anomalies of SST (K), precipitation (mm day^{-1}), the 500 hPa pressure height (m), and the equatorial ocean temperature averaged in 5°S–5°N (K) which are regressed onto the Niño3 index. Monthly anomalies with respect to monthly climatology are used here. From the left to the right, the anomalies in observations (ProjD and ERA-I), MIROC6, and MIROC5 are aligned. In the bottom panels, contours denote annual-mean climatological temperature with the 20°C isotherms thickened and the contour interval is 2°C.

Geosci. Model Dev. Discuss., https://doi.org/10.5194/gmd-2018-155
Manuscript under review for journal Geosci. Model Dev.
Discussion started: 16 July 2018

Geoscientific Model Development Discussions

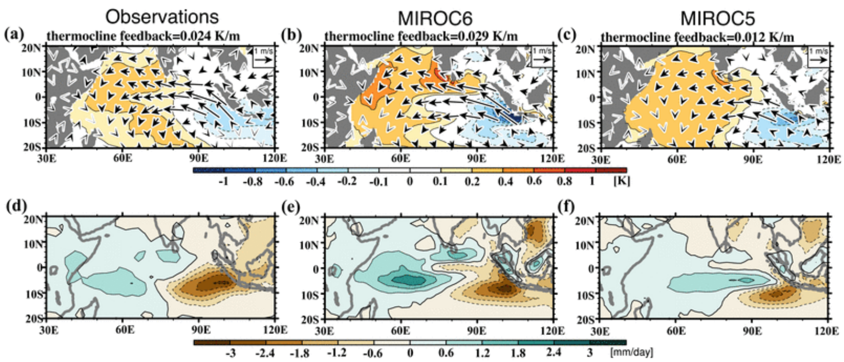

Figure 27. Same as Fig. 26, but for anomalies of SST (colors), 10 m wind vectors (upper panels) and precipitation (lower panels) regressed onto the autumn DMI. The values of the regression slope between anomalies of the 20°C isotherm depth and the SST over the eastern IOD region, which indicates the thermocline feedback, are displayed on the top of the upper panels.

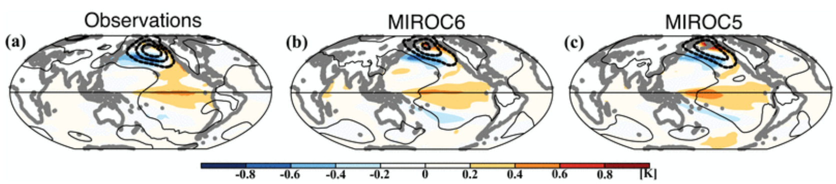

Figure 28. Same as Fig. 26, but for anomalies of monthly SST and wintertime SLP regressed onto the PDO index (see the text). COBE-SST2/SLP2 data in 1900–2013 are used as observations.

Geosci. Model Dev. Discuss., https://doi.org/10.5194/gmd-2018-155
Manuscript under review for journal Geosci. Model Dev.
Discussion started: 16 July 2018

Geoscientific Model Development
Discussions

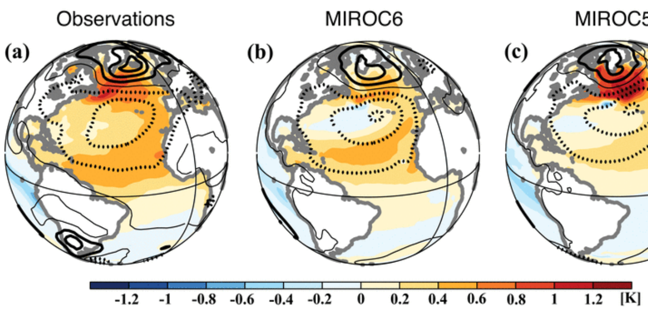

Figure 29. Same as Fig. 26, but for anomalies of SST (colors) and SLP (contours; 0.2 hPa) regressed onto the AMO index (see the text). Negative values are denoted by dashed contours.

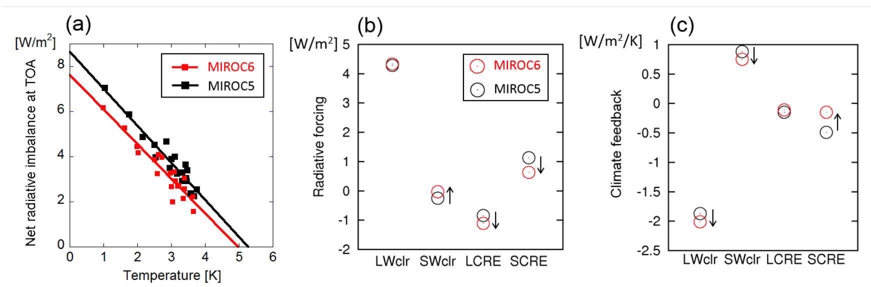

Fig. 30. (a) Global mean net radiative imbalance at the TOA plotted against the global mean SAT increase. Data from the first 20 years after the abrupt CO_2 quadrupling are used. (b) $2 \times CO_2$ radiative forcing estimated by regressing four components of TOA radiation against the global-mean SAT, following Gregory and Webb (2008). (c) Same as (b) but for climate feedback. In Figs. 30bc, LWclr (SWclr) and LCRE (SCRE) denote a clear-sky longwave (shortwave) component and a longwave (shortwave) cloud component, respectively. The arrows in (b) and (c) indicate that the results of MIROC6 are different from MIROC5 at the 5% level.

Geosci. Model Dev. Discuss., https://doi.org/10.5194/gmd-2018-155
Manuscript under review for journal Geosci. Model Dev.
Discussion started: 16 July 2018

Geoscientific Model Development Discussions

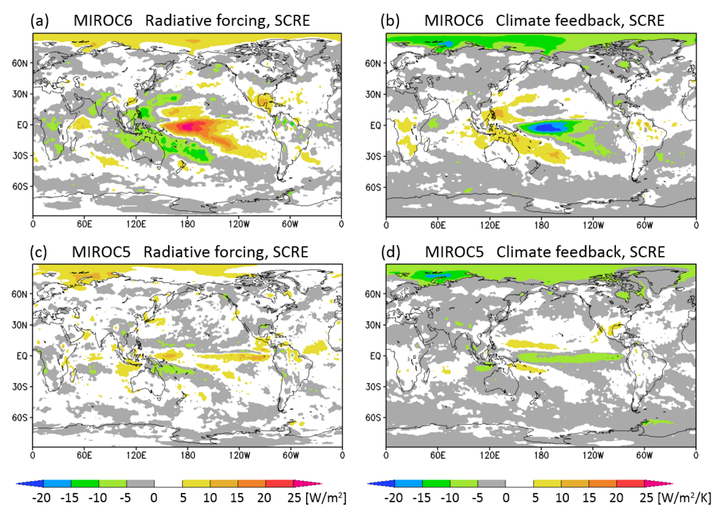

Figure 31. Shortwave cloud component of 2 × CO_2 radiative forcing (left panels) and climate feedback (right panels) in MIROC6 (upper panels) and MIROC5 (lower panels).

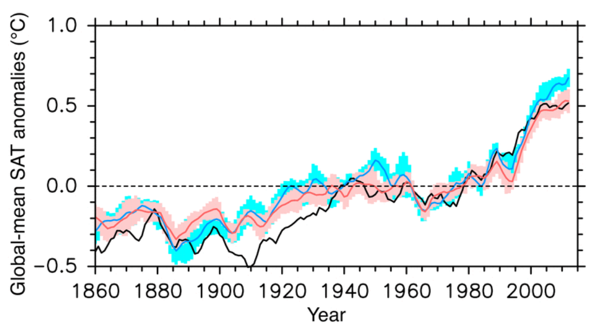

Figure 32. Time series of the global-mean SAT anomalies for observations (black), MIROC6 (red), and MIROC5 (blue). A 5-yr running-mean filter is applied to the anomalies with respect to the 1961–1990 mean. Colors indicate spreads of ensemble experiments for each model (1 standard deviation).

Geosci. Model Dev. Discuss., https://doi.org/10.5194/gmd-2018-155
Manuscript under review for journal Geosci. Model Dev.
Discussion started: 16 July 2018

Geoscientific Model Development Discussions
Open Access
EGU

Dataset	Used data period (year)	Reference
CERES (edition 2.8)	2001–2013	Loeb et al. (2009)
ISCCP	Climatology	Zhang et al. (2004)
ERA-Interim	1980–2009	Dee et al. (2011)
GPCPv2	1980–2009	Adler et al. (2003)
EASE-Grid 2.0	1980–2009	Brodzik and Armstrong (2013)
ProjD	1980–2009	Ishii et al. (2013)
SODA	1980–2009	Carton and Giese (2008)
SSM/I	1980–2009	Cavarieli et al. (1991)
NOAA OLR	1974–2013	Liebmann and Smith (1996)
COBE-SST2/SLP2	1900–2013	Hirahara et al. (2014)
HadCRUT	1850–2015	Morice et al. (2012)

Table 1. Summary of observation and reanalysis datasets used as the references in the present manuscript.

Model	ECS [K]	Radiative forcing [W/m^2]	Climate feedback [$W/m^2/K$]
MIROC6	2.5	3.81*	-1.53
MIROC5	2.6	4.33	-1.63

Table 2. Effective climate sensitivity (ECS), radiative forcing of CO_2 doubling, and climate feedback for MIROC6 and MIROC5. The result of MIROC6 with '*' is different from MIROC5 at the 5% level.

Geosci. Model Dev. Discuss., https://doi.org/10.5194/gmd-2018-155
Manuscript under review for journal Geosci. Model Dev.
Discussion started: 16 July 2018

Geoscientific Model Development Discussions
Open Access

Model	Radiative forcing [W/m^2]				Climate feedback [W/m^2/K]			
	LWclr	SWclr	LCRE	SCRE	LWclr	SWclr	LCRE	SCRE
MIROC6	4.33	-0.03*	-1.11*	0.63*	-2.01*	0.75*	-0.11	-0.15*
MIROC5	4.28	-0.25	-0.84	1.13	-1.87	0.88	-0.15	-0.49

Table 3. Radiative forcing of CO_2 doubling and climate feedback for MIROC6 and MIROC5, evaluated with different components of TOA radiation as longwave clear sky (LWclr), shortwave clear sky (SWclr), longwave cloud radiative effect (LCRE), and shortwave cloud radiative effect (SCRE). The results of MIROC6 with '*' are different from MIROC5 at the 5% level.

Geosci. Model Dev. Discuss., https://doi.org/10.5194/gmd-2018-155
Manuscript under review for journal Geosci. Model Dev.
Discussion started: 16 July 2018

Geoscientific Model Development Discussions
Open Access

Appendix

		MIROC5 (Watanabe et al., 2010)	MIROC6 (this issue)
Atmosphere	Core	CCSR-NIES AGCM (Numaguti et al., 1997)	Same as MIROC5
	Resolution	T85 (150 km), 40 levels up to 3 hPa	T85 (150 km), 81 levels up to 0.004 hPa
	Cumulus	An entrainment plume model with multiple cloud-types (Chikira and Sugiyama, 2010)	Same as MIROC5
	Shallow conv.	N/A	A mass flux-based single plume model based on Park and Bretherton (2009)
	Aerosol	SPRINTARS (Takemura et al.,2000, 2005, 2009)	Same as MIROC5, but with prognostic precursor gases of organic matters and diagnostic oceanic primary and secondary organic matters.
	Radiation	*k*-distribution scheme (Sekiguchi and Nakajima, 2008)	Same as MIROC5, but with a hexagonal solid column as ice particle habit and extended mode radius of cloud particles.
	Gravity waves	An orographic gravity wave parameterization (McFarlane, 1987)	Same as MIROC5, but with a non-orographic gravity wave parameterization (Hines, 1997)
Land	Core	MATSRIO (Takata et al., 2003)	Same as MIROC5, but with parameterizations for subgrid snow distribution (Linston et al. 2004; Nitta et al., 2014) and a snow-fed wetland (Nitta et al., 2017)
	Resolution	T85 (150 km), 3 snow layers and 6 soil layers down to 14 m depth	Same as MIROC5
Ocean/sea-ice	Core	COCO4.9 (Hasumi, 2004)	Same as MIROC5
	Resolution	Nominal 1.4° (bipolar grid system), 49 levels down to 5500 m	Nominal 1° (tripolar grid system), 63 levels down to 6300 m
	Turbulence	1.5 level turbulent closure model (Noh and Kim, 1999)	Same as MIROC5, but modified turbulent kinetic energy input and smaller background vertical diffusivity under sea-ice (Komuro 2014)

Table A. Summary of the updated configurations from MIROC5 to MIROC6